Mechanical behaviour and machining of nanocomposites

2.1 Introduction:

The aim of this chapter is to investigate the machinability of two different nano-composite materials (Jute fiber, Glass fiber/epoxy and Jute fiber, Glass fiber/graphene/epoxy) in terms of Material removal rate when slot micro-milling. Experimental design is performed using Taguchi's L_9 orthogonal array. A number of performance factors, including material removal rate, are taken into account while optimising machining process parameters including feed rate, tool cutting speed, cutting environment (dry), and depth of cut. The significant parameter are discovered using ANOVA. Benefiting from the high specific surface area of the Nano-composite $(0^0,0^0,0^0,0^0)_S$ = 2818 m^2/g, this material could act as an adsorbent. The thermal properties and flame retardancy of both hybrid composite $(0^0,0^0,0^0,0^0)_S$ and $(0^0,30^0,45^0,60^0)_S$ and nano-composite $(0^0,0^0,0^0,0^0)_S$, were investigated, and the possible flame retarding mechanism was proposed. The current study also looked at how two-dimensional nanoscale inclusions affected the way jute-glass hybrid composites responded to low-velocity impacts based on ASTM specifications. These nanomaterials differ in terms of their chemical composition, toughness, and surface energies (organic and inorganic forms, graphene, respectively). The bonding strength and physical defects on the surface of plain composites and nano-composites were analysed using a scanning electron microscope (SEM).

2.2 Materials and composite fabrications

2.2.1 Material details

The current study used Glass fiber and jute fiber as a continuous-fiber reinforcement fabric. This 560 GSM – Woven Glass Fabric 5H Satin has a "warp 24.0 ends/inch" and "weft 24.0 picks/inch". The diameter of the filament is 13µm for glass fiber and jute fiber. Araldite LY556 is used as epoxy resin and HY951 as a hardener. This matrix is cured at room temperature. LY556 is a bi-functional resin and HY951 is an aliphatic primary amine. The mixing ratio is 10:1 weight-to-weight. Epoxy adhesives are a significant component of the category of adhesives known as "engineering adhesives" or "structural adhesives" (which also contains acrylic, polyurethane, cyanoacrylate, etc.) These high-performance adhesives are utilised in manufacturing cars, trucks, bikes, golf clubs, skis, snowboards, and other items where strong bonding is necessary. Multi-layer graphene with a purity of more than 90% is one of the nanomaterials chosen as inclusions for the composite. There are 6–10 layers in these graphene films. Their dimensions range from 10 to 50 m and are 3 to 8 nm thick. The graphene that was purchased was a fine, grayish-black powder with an average density of 2.2 g/cm^3. Figure 2.26 shows the scanning electron microscopy (SEM) of the pristine graphene nanoflakes.

2.2.2 Diffusion of Nano-filler in Epoxy

In a beaker, pure graphene and epoxy resin were combined at the predetermined weight ratio before adding the curing agent. Using an ultra sonicator, the material was extensively stirred for two hours. Next, a 3:2 ratio of the curing agent was poured to the beaker while being manually agitated with a glass rod. To eliminate the bubbles produced during the mixing, the

resin was degasified in a vacuum chamber.

2.2.3 Fabrication of hybrid composites and Nanocomposites

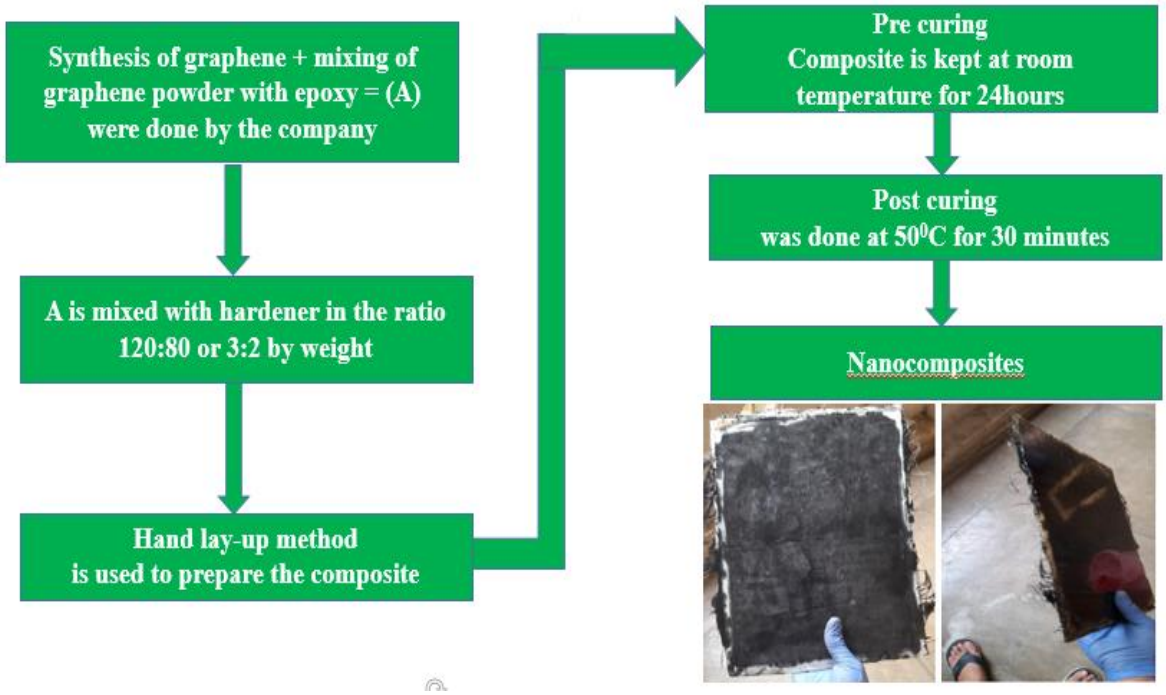

Figure 2.1. Flow chart for the synthesis of nanocomposites.

A total of 60 fibre-reinforced epoxy hybrid composite and 30 nanocomposite samples with eight plies were fabricated using the hand lay-up process. As reinforcement, glass and jute fibres were employed, while the epoxy was chosen as the matrix material. The layers of fibre are added one after the other, beginning with glass fibre, followed by jute fibre, again glass fibre, and so on. Epoxy resin that cures at low temperatures was blended with hardener in a ratio of 10:1 weight percent in hybrid composites and 3:2 weight percent in graphene-based hybrid composites. The mould surfaces was first treated with a releasing agent. A sheet of glass fibre was then added, after which a considerable quantity of matrix were added on top of it. To fill up any spaces inside this fabric structure and evenly distribute the resin through-out the fibres, brushes and hand rollers were used.

Up until the required number of layers were added, the procedure was repeated. The initial curing method was carried out in a hydraulic press with a 2 MPa uniaxial pressure over at room temperature for 24 hours. During the compression moulding process, excess epoxy resin as well as some reinforcing fillers were removed. The real reinforcement densities may therefore be a bit lower than that of the desired values as a result of the tiny filler dimensions of the graphene-reinforced specimens. The material properties are shown below:

Table 2.1. Properties of the constituent material.

	Young's modulus (E) GPa	Poisson's ratio (μ)	Modulus of rigidity (G) GPa	Mass Density (ρ) g/cm^3
E-glass fiber	80	0.25	32	2.62
Matrix	2.915	0.3	1.121	1.15
Jute fiber [142]	10-30			1.5

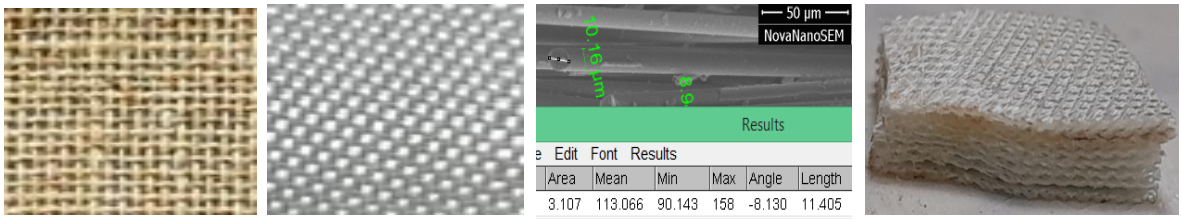

(a) (b) (c) (d)

Figure 2.2. (a) Woven Jute fiber mat, (b) Woven glass fiber mat, (c) Diameter of fiber calculated from SEM result (=10.16 micron) and with the help of software (=11.405), (d) A burn-out tested sample.

Now the hybrid composite plate is ready, but in case of graphene-based hybrid composites, post-curing is needed. So, the partially-cured composites were then placed in an oven set at 50 °C for 30 minutes to finish the curing process. In the case of a hybrid composite, post-curing is not needed. Finally, the composite plate was cut for five tensile test specimens,

twenty impact test samples, five for each notch, and five samples for checking machinability. The fabricated composites are: (i) Hybrid composite with zero degrees ply orientation $[H.C.]_0$, (ii) Hybrid composite with different stacking sequence $[H.C.]_A$, and (iii) Nano Hybrid composite with zero degrees ply orientation $[NHC]_0$. The stacking sequence of angle is 0^0-30^0-45^0-60^0-60^0-45^0-30^0-0^0.

2.3 Characterizations and measurement

2.3.4 Resin Burning-off Method

The volume fraction can be estimated using the initial weight of the composite and the weight of the fibres by heating the composite to a temperature where the resin will melt but the fibres

Table 2.2. Volume fraction of different composite

Composite types	Experimental	Theoretical
Hybrid (Zero degree)	52.06	50
Hybrid (Angled)	52.06	50
Nano-Hybrid (Zero degree)	46.23	45

will remain stable, burning off the resin, and weighing the fibres. The mass fraction of plain composite is 52%, and for nano-hybrid composite, it is less than 45% as per ASTM standard 2584 [143]. The mass fraction is calculated by applying the burn-off method as per ASTM 2584 [143].

2.3.5 Thermal Stability of Polymer Nanocomposites

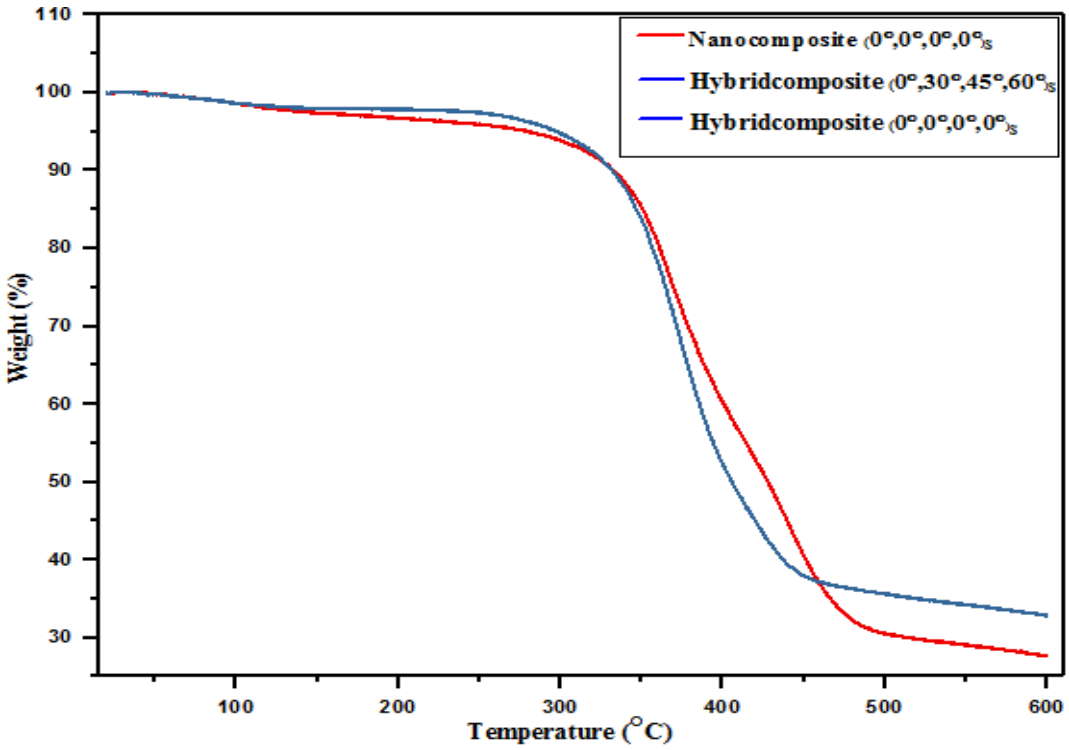

Figure 2.3. TGA curves of hybridcomposite and its nanocomposites

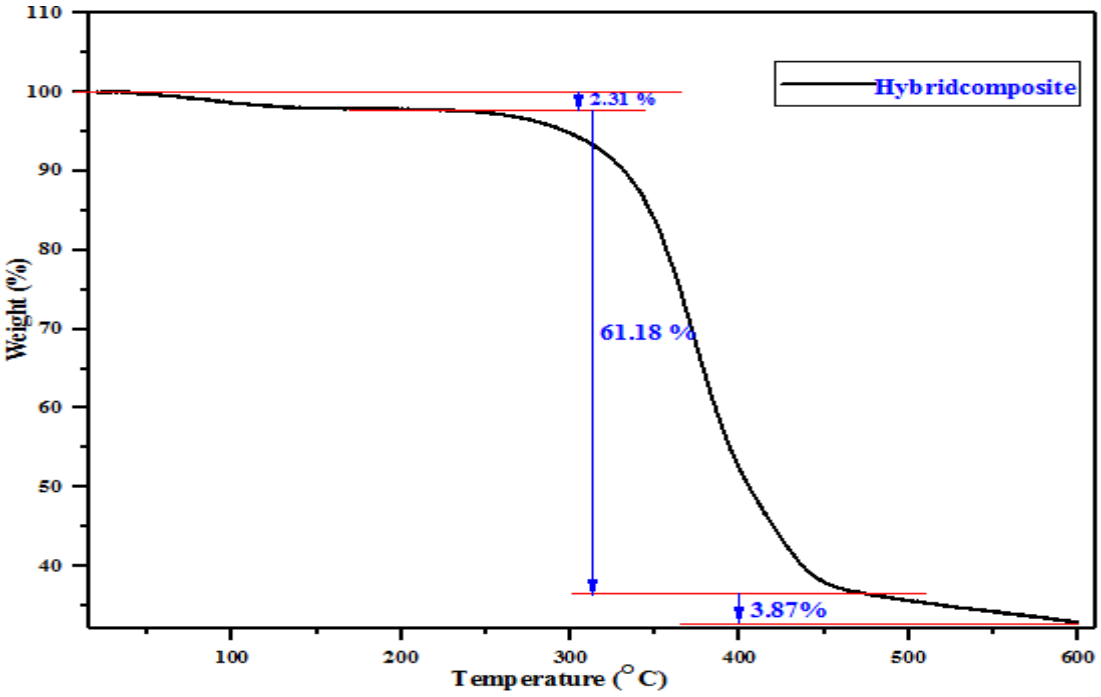

Figure 2.4. TGA curves of hybridcomposite.

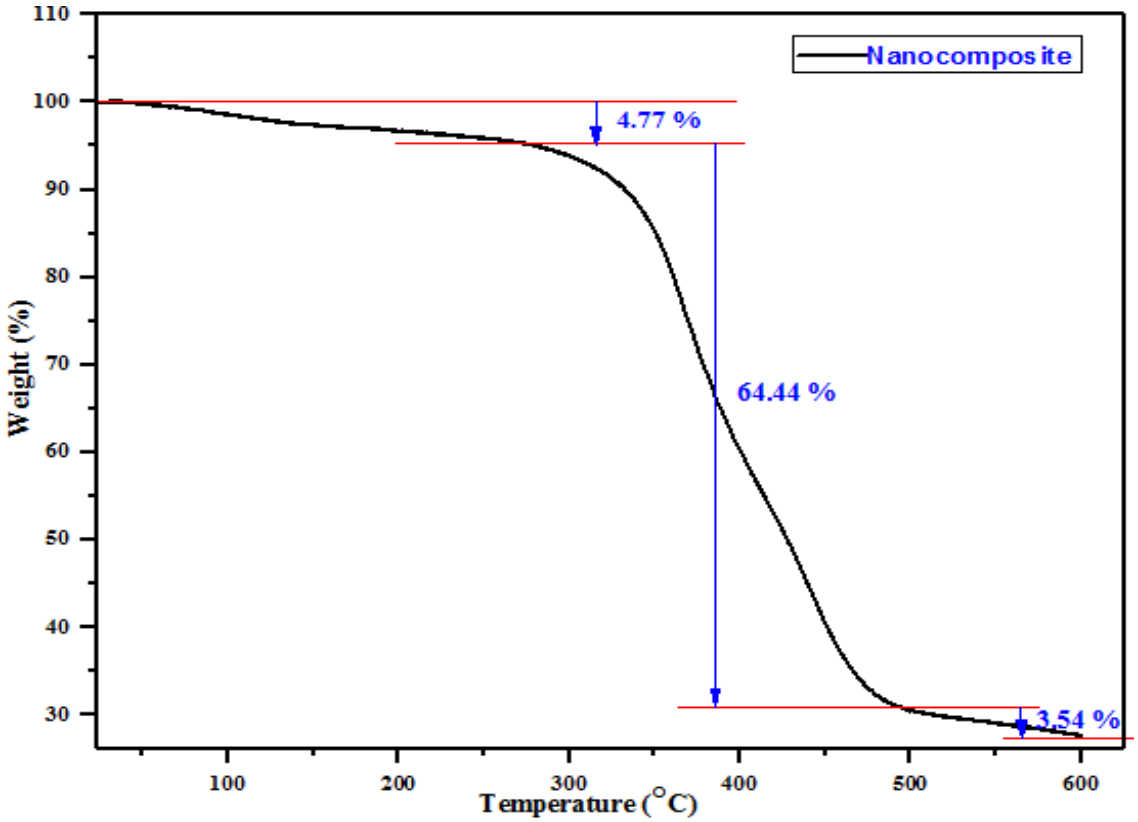

Figure 2.5. TGA curves of nanocomposites

Table 2.3. Calculation of specific surface area for the use of this materials as an adsorbent

Serial number	Composite	Specific surface area (m^2/g)
1	Hybridcomposite $(0^0,0^0,0^0,0^0)_S$	2612
2	Hybridcomposite $(0^0,30^0,45^0,60^0)_S$	2612
3	Nanocomposite $(0^0,0^0,0^0,0^0)_S$	2818

The performance of polymer materials during combustion is highly correlated with their thermal degradation characteristics. The thermal degradation behaviour of polymer materials has been extensively studied using TGA [25–27]. The thermal gradient analysis (TGA) method was used to assess hybrid composites thermal stability and degradation characteris tics and the associated nanocomposites. Thermal degradation occurs in one stage for a neat hybrid composite having 28% nanocomposite material and 33% hybrid composite material

still at 600°C, respectively. In comparison to nanocomposite $(0^0,0^0,0^0,0^0)_S$, both hybridcomposite $(0^0,0^0,0^0,0^0)_S$ and $(0^0,30^0,45^0,60^0)_S$ exhibit similar degradative behaviour. However, hybridcomposite samples shows excellent thermal stability, as evidenced by the weight (%) loss of 2.31% for hybridcomposite and 4.77% for nanocomposite from 0^0C to 250^0C. The increased residue of 33% hybrid composite and 28% nanocomposite at 600°C provides additional evidence of better thermal stability. The thermal stability of hybrid composites is superior to that of nanocomposites up to 350^0C and between 450^0C and 600^0C. The primary causes of the increased thermal stability between temperatures of 350^0C and 450^0C are the so-called tortuous route effect of nanosheets, delay in escaping volatile degradation products, and the creation of extra char residues. Graphene addition does not affect the pace at which a nanocomposite degrades, in contrast to the change in heat stability

2.3.6 Measurement of the porosity

Table 2.4. Calculation of Apparent porosity of different composite material.

Serial no	Composite Type	Apparent Porosity (%)
1	GFRP	9.04
2	Hybridcomposite $(0^0,30^0,45^0,60^0)_S$	6.43
3	Hybridcomposite $(0^0,0^0,0^0,0^0)_S$	9.21
4	Nanocomposite $(0^0,0^0,0^0,0^0)_S$	7.93

All of the specimens that were used for the measurement comparison were taken from the same uni-directional plate. To produce a porosity that was as typical of the plate's total porosity as feasible, the specimens were sliced at several spots. The specimens' lengths are in line with the direction of the fibres, and their widths are perpendicular to the directions of

thickness and length. There were three different kinds of porosity measurements used (visual, mechanical and gravimetric). The visual approaches involve measuring the surface or volume percentage of the voids and getting 2D pictures or 3D volumes of the interior structure of the composite. The mechanical technique entails performing an inverse identification of the volume of voids inside specimens subjected to tensile testing in order to determine the impact of porosity on the mechanical characteristics of the composite. In order to calculate the specimens' porosity and to establish their fibre volume fraction (FVF), gravimetric measurements entail weighing the specimens and their components under various situations.

2.3.7 Density and specific gravity of composites by displacement method

Density, which is measured in accordance with ASTM D1895 standards and is described as the mass of the material per unit volume [147], represents one of the most important factors in determining the properties of polymer composite materials. Its worth in polymer composites mainly relies on the reinforcement to matrix ratio. The density of the composite constituents is determined by comparing the weight of a sample measured in air and then again while suspended on a wire and submerged in water (fibres and matrices). When the specimen's density is less than that of water, a sinker may be attached with a wire to make immersion easier. Equation *(2.1*) is then used to compute the density.

$$\rho = \frac{(0.9975)a}{(a + w - b)} \qquad (2.1)$$

Where a represents the weight of the specimen in the air, b represents the combined weight of the specimen and sinker when fully submerged, and the weight of the wire while partially submerged is represented by w. Similar principles are used to determine a composite's den

sity. In some circumstances, the ASTM D1895 standard is used to assess composite density, and equation (2.2)

$$Density\ (g/cm^3)\ = \frac{m}{v} \qquad (2.2)$$

where m denotes the composites' mass and v denotes their volume.

Table 2.5. Calculation of density of different composite material using archimedes principle.

Serial no	Composite Type	Density (g/cm^3)
1	Glass fiber polymer composite $(0^0,0^0,0^0,0^0)_S$	1.4764
2	Hybridcomposite $(0^0,30^0,45^0,60^0)_S$	1.3199
3	Hybridcomposite $(0^0,0^0,0^0,0^0)_S$	1.2562
4	Nanocomposite $(0^0,0^0,0^0,0^0)_S$	1.2185

2.4 Mechanical property

2.4.1 Tensile Test

Tensile testing is a destructive test method that reveals details about the tensile property of different materials such as UTS, modulus of elasticity, ductility etc. It measures the force required to fracture a composite sample as well as the amount of stretch or extension that happens prior to that. The tensile strength of composite materials is typically evaluated using basic tension or flat-sandwich tension testing in line with standards like ASTM D 638 or ASTM D 3039. These investigations produce stress-strain diagrams, which are then used to calculate the tensile modulus.

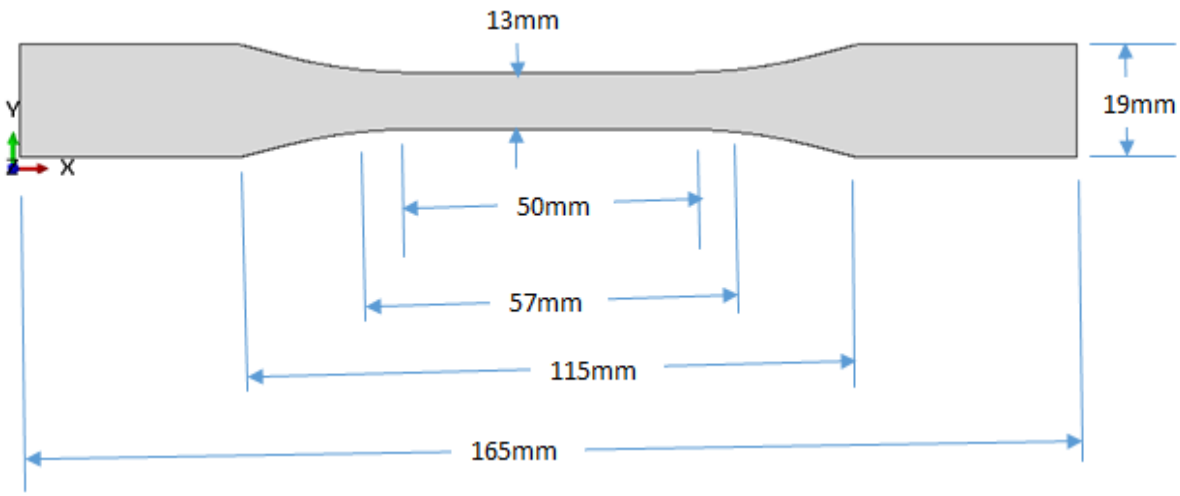

Figure 2.6. Tensile Specimen dimension as per standards ASTM D 638 type-I

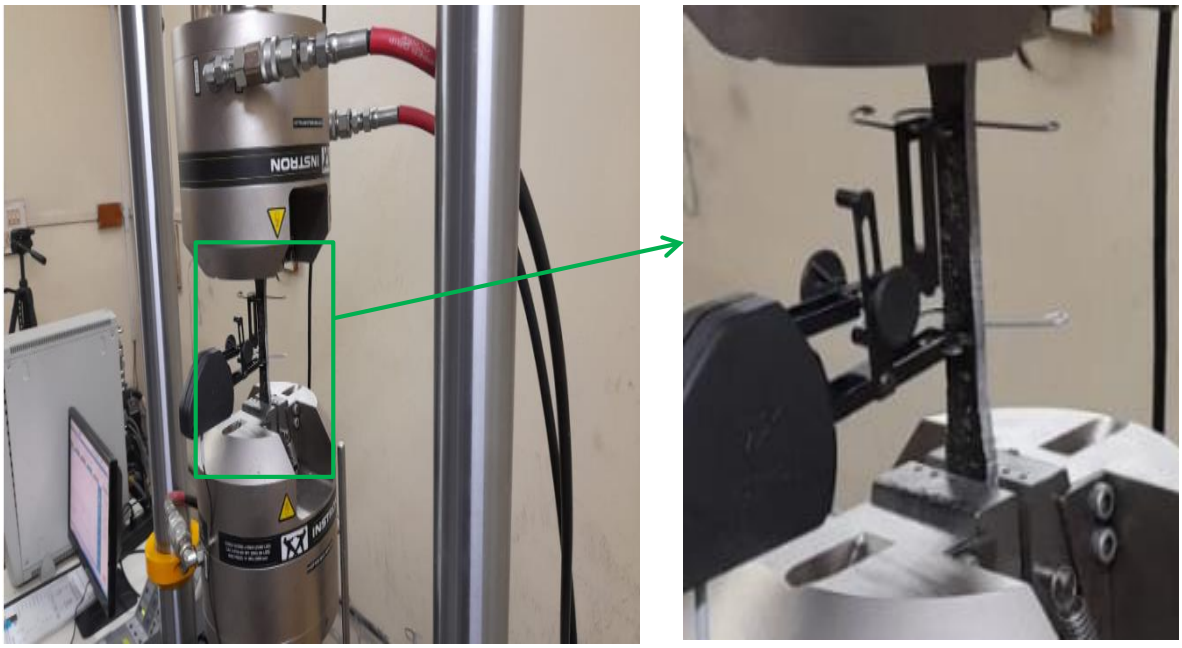

Figure 2.7. Tensile test set-up for investigating the tensile property of nano- composite

Figure 2.7 shows tensile testing where ASTM D 638 technique is used to assess the tensile behavior of composites with universal testing equipment, Instron capacity 1–100 KN where 1 mm/min is the chosen strain rate. Additionally, the results of tensile testing include the following measurements: UTS (either at yield point or at breaking point), modulus of elasticity, percentage strain, percentage elongation at yield and elongation at break.

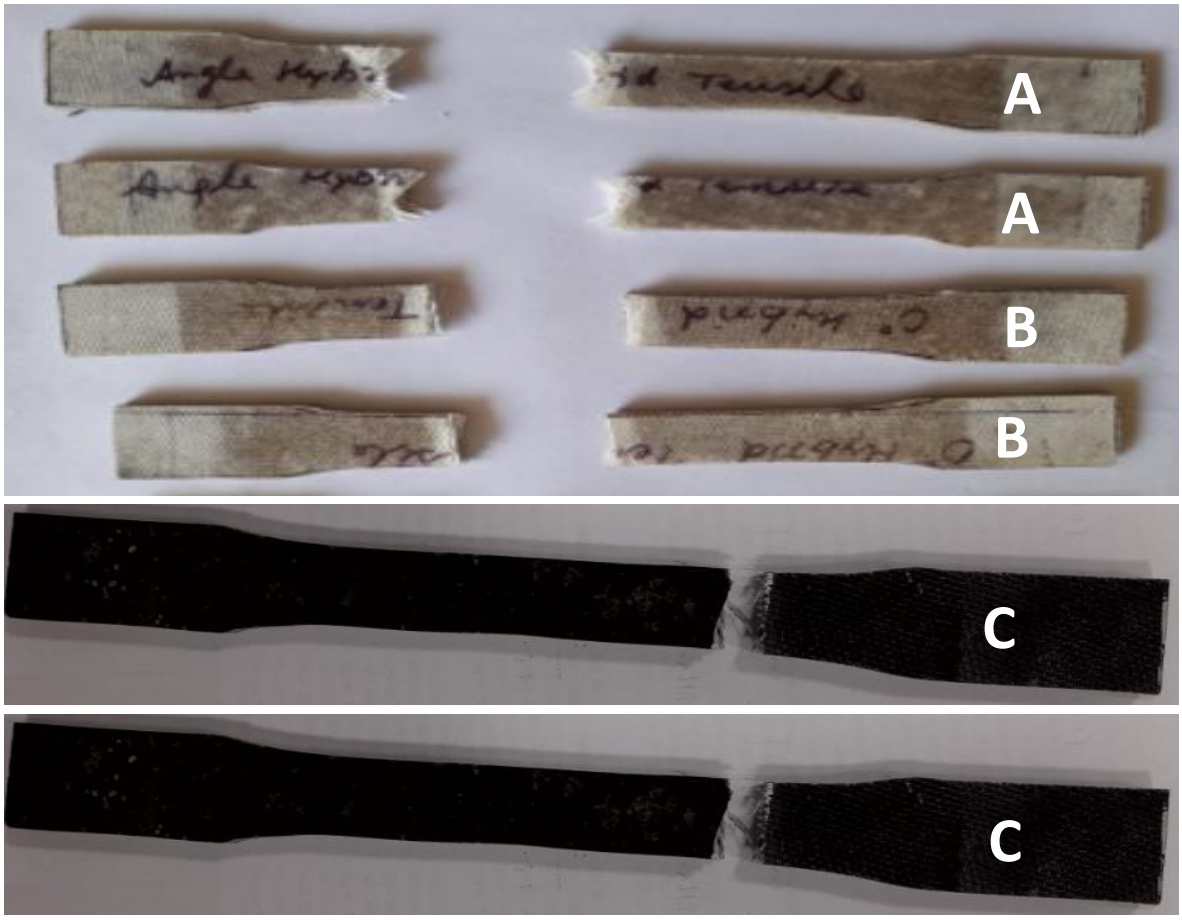

Figure 2.8. Specimen for Tensile test as per standards ASTM D 638 A: Hybrid composites $(60^0,45^0,30^0,0^0)_S$ B: Hybrid composites $(0^0,0^0,0^0,0^0)_S$ C: Nanocomposites $(0^0,0^0,0^0,0^0)_S$

Plain composite laminates are most frequently tested under in-plane tensile conditions. Furthermore, tensile tests are also conducted on portions of sandwich core materials, through thickness specimens, and bundles of fibres that have been resin-impregnated (also known as "tows"). Due to the anisotropy of composites, which causes different characteristics and strengths Alignment is crucial for composite testing implimentation dependent on the direction of the applied load. The tensile properties of a composite material is thus significantly decreased when tested in a position other than parallel to the fiber direction. Interesting is the use of composites in high-tensile-stress structures in the aircraft industry. Considers better axial load-string alignment during the tensile test in order to establish the maximum tensile strength in the fibre direction. For testing at temperatures between 2690^0C and 6000^0C, there

are currently several trustworthy gripping methods available, such as conventional actuation, hydraulic actuation and pneumatic actuation.

2.5 Impact test

The goal of the impact test would be to determine how such a sample of a known material, like polymer reinforced composites, would respond to a sudden increase in stress. Engineering materials' resistance to high-rate loading, including their brittleness, notch sensitivity, hardness, and impact strength are specifically assessed using the impact test [148].

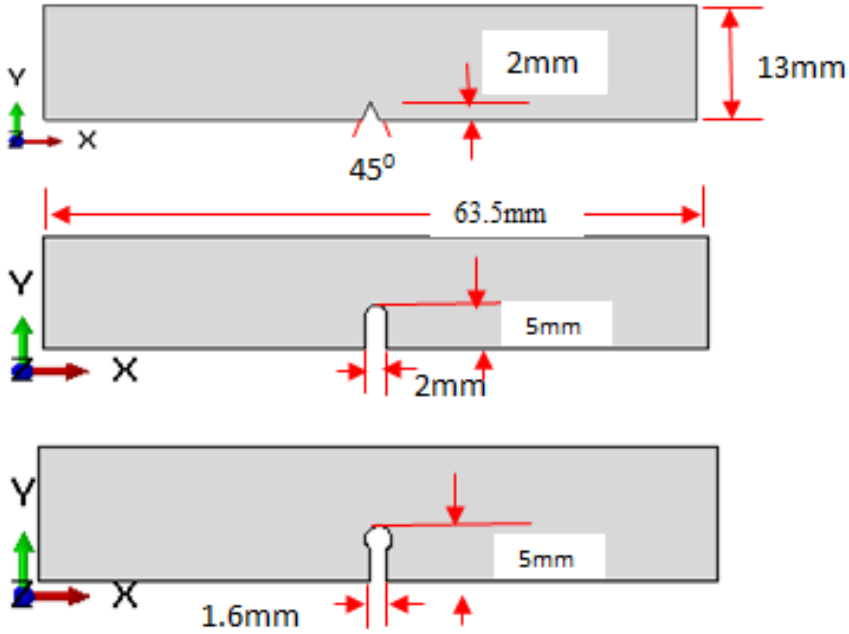

Figure 2.9. Different notches of impact test

In terms of product liability and safety, the ability to measure the impact property is quite advantageous. There are several notch configurations for impact test samples, such as V-notch, U-notch, key-hole, and no notch. The most commonly used sample configurations for impact testing are Charpy and Izod. In contrast to the Charpy impact test, the Izod impact test places the notch toward the striker. As a consequence, the specimen in the Izod test stands straight up like a fence post, as opposed to the Charpy test where the test piece is held hori

zontally between two vertical bars. However, the steel casting industries frequently employ the keyhole-shaped notch, which is assessed in the same manner as the "V" and "U" notches in the keyhole impact test. Figure 2.9 shows the Key-hole notch, the V-notch, and the U-notch. Where the material thickness is constrained, keyhole impact testing is often conducted at cryogenic temperatures. Impact testing tools were selected in accordance with ASTM standard D256 to ascertain the impact strength of the fibre. The test specimens (63.512.73.17 0.45 mm^3) were machined in accordance with ASTM standards. The CEAST resil impactor of energy 5.5 J with a tester in the pendulum type was used to conduct the impact test and it is shown in Figure 2.10. It is specifically made for testing impacts with energies ranging from 1 to 25 J. The difference between the impactor's initial and final heights represents the energy lost during specimen fracture. The specimen fractured as a result of the force of the pendulum coming down from a 1350-foot height. During the experiment, the composite's energy absorption was measured and examined. With the use of the following equation (2.3), the total amount of energy needed to break the specimen is calculated

$$E_T = mg(h_0 - h_f) \pm 0.2J \quad (2.3)$$

Where $E_{.T.}$ =Total energy; g = acceleration due to gravity; m = mass; h_0 = initial height and h_f = final height.

The impact strength or resilience is defined as total absorbed energy per unit cross-sectional area (kJ/m^2) following the ASTM standard D256

$$E_C = \frac{E_T}{wt} \quad (2.4)$$

Where t = thickness and w = width of specimen. The energy losses owing to air resistance have been taken into account. However, other losses due to bearing friction are neglected due to their small magnitude.

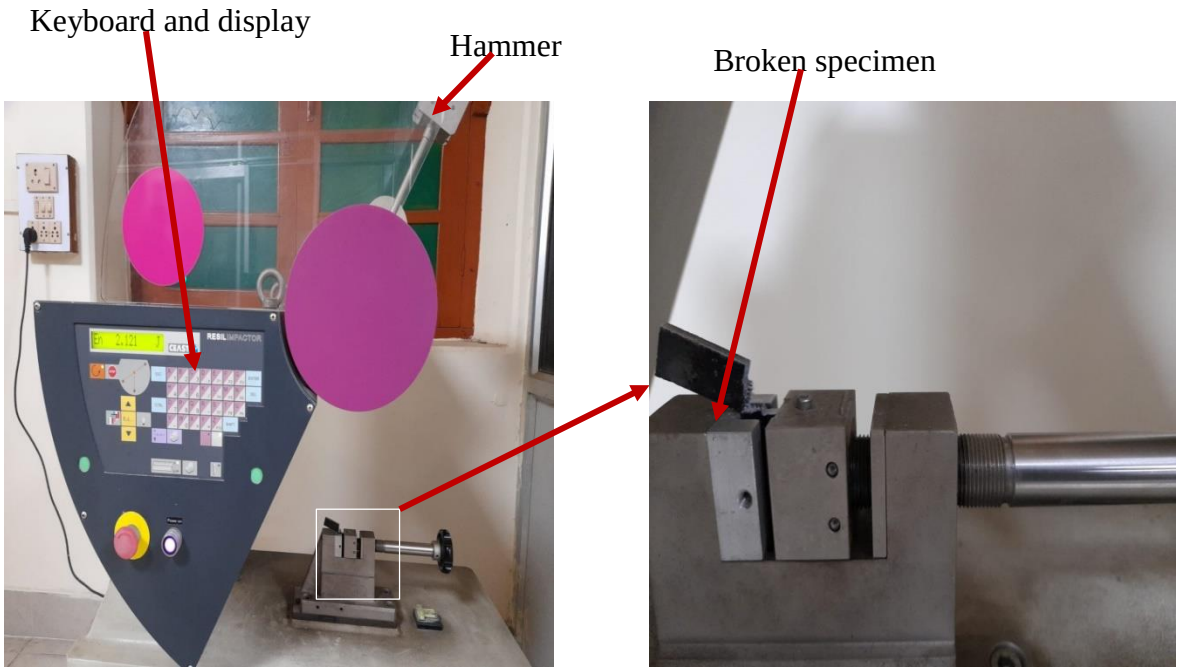

Figure 2.10. Resil impact test set-up for investigating the impact behavior of composite.

2.6 Results and discussion

Tensile, impact, and machining characteristics are used to examine the influence of nano-fillers on the mechanical behavior of nanocomposites. Figure 2.12 depicts the influence of nano-fillers on the tensile behavior of nanocomposites. Table 2.6 shows the precise tensile behavior of the composites examined. Tensile strength and % elongation are used to investigate this phenomenon. The mechanical behavior of zero-degree hybrid composites $[H.C.]_0$ is the best among the composites examined, as seen in the figure. Hybrid composites $[H.C.]_0$ demonstrated a tensile strength of 164.18 MPa. This is because composites contain high strength and modulus of J.F. and G.F. This is intended for composites where the combined impact of G.F. and J.F. is larger than the individual effect [149]. Furthermore, the slenderness ratio of both fibres enhanced the hybrid composites' tensile strength.

Table 2.6. Tensile properties of different types of composites

Properties	ASTM standard	Plain Hybrid composite		Nanocomposite
		$[HC]_0$	$[HC]_a$	$[NHC]_0$
Max. elongation (mm)	ASTM D638	2.101	2.19352	2.717203
Peak load (N)	ASTM D638	7470.31	5002.189	7407.379
Stiffness (N/mm)	ASTM D638	3555.6	2280.44	2726.104

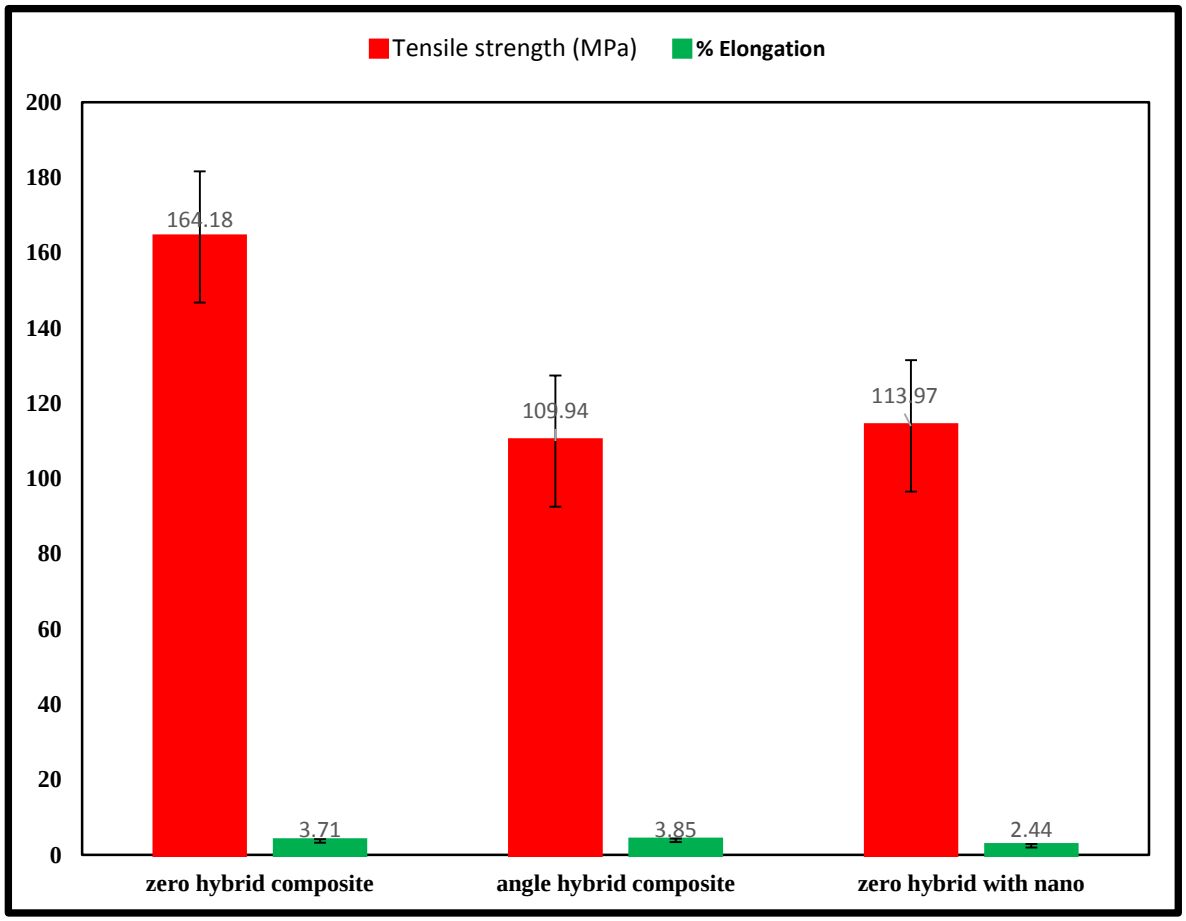

Figure 2.11. Effect of nano-fillers on tensile behaviour of nanocomposites

The matrix surmounts the fibres are more because of the large surface area of fibre which allows for the formation of strong adhesive bonds between the matrix and fibres [150]. $[H.C.]_A$'s tensile strength has been reduced by 33% to 109.94 MPa because of the effect of the orientation of fibers which is affecting the load-sharing capacity of fibers.

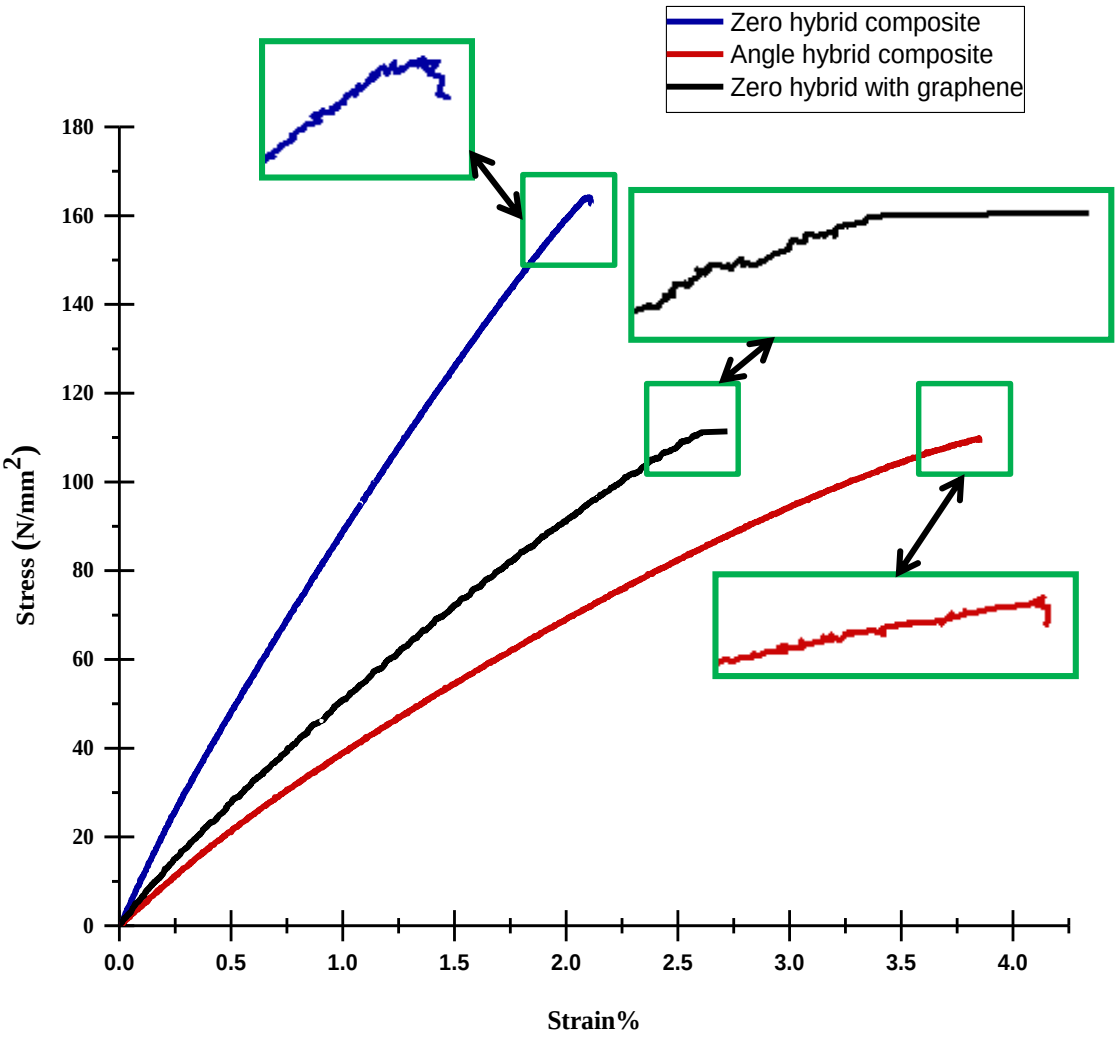

Figure 2.12. Stress–strain plot describing of a tensile behavior of nanocomposite.

Another reason is the inadequate interfacial bond among the fillers in a matrix. A filler might become stuck between the hybrid fibres, preventing resin from entering the surface as a result of which voids form [150]. The strength of nanocomposites was also reduced as a result of the fillers' different molecular weights [151]. Furthermore, the reinforcement makes the polymer more brittle by immobilising macromolecular chains. As a result of the aforementioned factors, nanocomposites lose their tensile strength. This is consistent with other people's work [137, 138]. The presence of nano- fillers noticeably degraded the tensile properties of nano

composites. Tensile data of the material have been reduced to 113.97 MPa this is a 31% reduction in strength compared to $[H.C.]_0$. This demonstrated that the hybrid effect with fibre is more favorable compared with the hybrid effect using nano-filler. When comparing the promotion of strength employing fillers, nano-fillers contribute to a decrease in strength [152]. The synergy between hybrid fillers in composites has been observed. Nanocomposites have shown a slight change in the strength of 31% compared to $[H.C.]_0$. The nano-fillers are to blame for the poor strength loss. This has shown how nano-fillers affect composite tensile strength. Nano additives result in a reduction of the strength of composites. They also encouraged the agglomeration of nanoparticles in resin-free flow areas. Nano-filler decreases the strength by restricting molecular chain mobility, causing the improvement in crystallinity of nanocomposite [153]. The application of nano-fillers improves the interface between fiber and matrix of nanocomposites. This is because of the formation of a percolation network among composite reinforcements due to the addition of nano-fillers [154], nanocomposites lose their strength as a result of this. One of the primary causes for the weakening of nanocomposites is the nanoparticle aspect ratio. Because of the geometrical differences between fillers and fibers, voids form, reducing the mechanical properties of nanocomposites [141, 143]. Because of the difference in the nano-size of additives, the degree of agglomeration of nano-fillers is enhanced. Furthermore, fillers efficiently cover the overlapping space between hybrid fibres. Because of their effective surface area, nano-fillers have strengthened the surface contact between the partners of nanocomposites. Calculated results are consistent with the previous research [156]. Figure 2.11 shows the synergistic effect of nano-fillers on the percentage elongation of composites. $[H.C.]_A$ hybrid composites have a percentage elonga tion of 3.85. Brittle nature and reduction in elasticity results in a decrease in ductility [153]. The influence of orientation improves composite ductility. It is 3.85 out of 3.71 for hybrid

composites. This is because of the influence of an increment in the brittleness of composites. Non-resin flow zones can also be seen at the interface of hybrid fibres. During load transformation, these locations were subjected to extreme stress concentration [145, 146]. This could lead to material failure at an early stage. However, nano-fillers reduced the ductility even further. This might be the result of stress concentration and agglomeration at matrix and fiber interfaces; as a result, adding nano-fillers to nanocomposites reduces their ductility. It is 3.17 out of 3.85 for hybrid composites. Figure 2.12 shows the stress-strain curve of the composites examined. In comparison to $[H.C.]_0$ hybrid composites, the nanoparticle additives lowered the load-carrying capability and strength of nanocomposites even more. This might be because composites are becoming less ductile. However, among the composites investigated, the strain resistance of hybrid composites with good ductility was higher. The enhanced degree of porosity in nanocomposites may disrupt the network of adhesion between fillers, resulting in a reduction in strain [158].

2.6.1 Impact property

When the impactor makes contact with the specimen, the load will suddenly rise. The number of oscillations near the peak load is more because of internal damage like delamination, matrix cracking and fiber breakage. After the complete fracture of the specimen took place, the load slowly drops to zero, and the specimens were separated from the impactor. For better clarity about the impact performance of graphene-reinforced composite, the analysis shows the lowest peak load for plain composite and large displacement. The graphene-reinforced CFRP composite has a peak load of 2.48 kN; there is only a 2.1% difference between the unreinforced composite and the addition of In terms of impact resistance, graphene provided slight improvement. The effect on impact property can be categorized into two group's

namely (i) the Effect of different reinforcement and (ii) Notch sensitivity.

2.6.1.1 Izod impact

Like the Charpy impact test, the Izod impact test evaluates materials at low temperatures. In this test, a specimen is made into a square or circular slice with one, two, or three notches that have the dimensions 63.5 mm × 12.7 mm × 3.17 mm [148]. In the Izod impact test, the specimen is firmly held vertically while a pendulum with a weighted end swings down and strikes it. The pendulum's energy loss, as measured exactly by the height lost throughout the swing of the pendulum, determines the impact strength. Impact strength was also described by researchers as the capacity of polymer composites to withstand highly energetic impacts without cracking or breaking. Additionally, they said that the impact properties of fiber-reinforced polymer composites and hybrid composites are determined by the characteristics of the individual fibres employed for hybridization, interlaminar adhesion, and interfacial adhesion between the fibre and the matrix [148].

2.6.1.2 Effect of different reinforcement

The calculated results, as shown in Figure 2.13 reveal that $[H.C.]_A$ has the least energy absorption capacity, $[NHC]_0$ has 3.04% more and $[H.C.]_0$ has the highest energy absorption capacity composite in the case of U-notch because composites have stiff and rigid fibres. The inclusion of graphene minimized energy absorption capacity by 7.25% in the case of U-notch it is because of the presence of nanofillers and the effect of stress concentration. Whereas in the case of V-notch $[H.C.]_0$ having the least energy absorption capacity, $[H.C.]_A$ has 3.23% more and $[NHC]_0$ is the highest energy absorption capacity composite. The inclusion of gra phene maximized the energy absorption capacity by 10.27% in the case of V-notch; here,

notch help nullify the effect of stress concentration, improving energy absorption capacity.

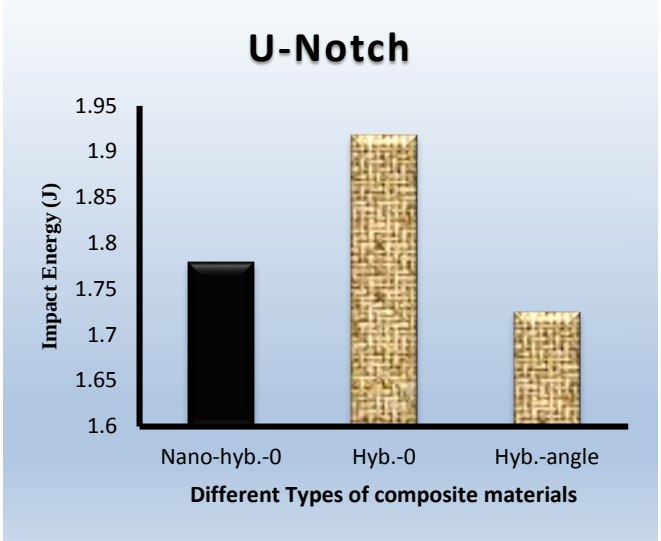

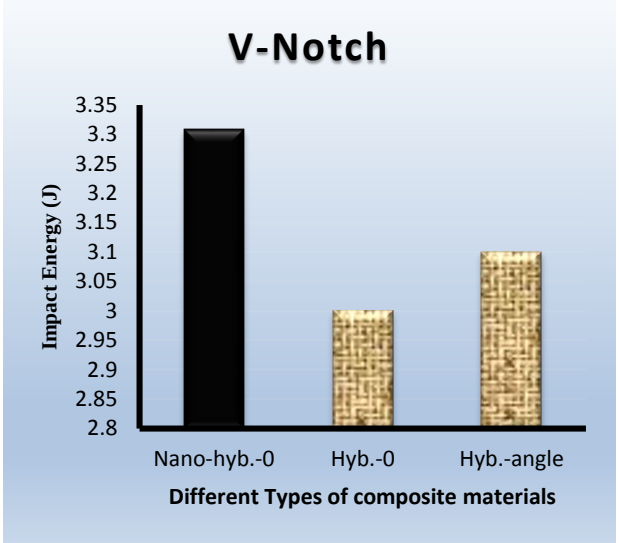

(a) -7.25% decrement in case of $[HNC]_0$ vs

(b) +10.27% increment

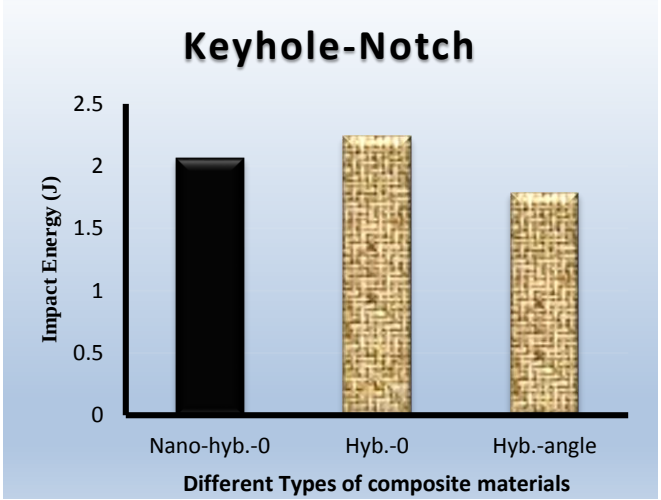

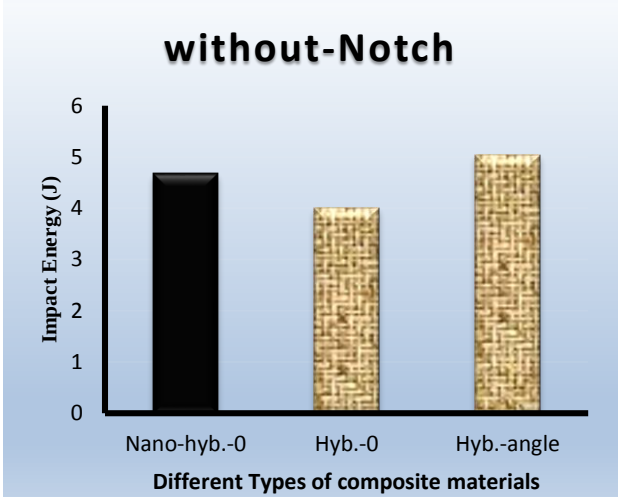

(c) -7.77% decrement

(d) +16.8% increment

Figure 2.13. Energy absorption charts showing the effect of different reinforcement.

In the case of Key hole-notch $[H.C.]_A$ having the least energy absorption capacity, $[NHC]_0$ has 13.57% more, and $[H.C.]_0$ has the highest energy absorption capacity. The inclusion of graphene minimized energy absorption capacity by 7.77%. In the case of the notch-free spec imen, $[H.C.]_0$ has the least energy absorption capacity, $[NHC]_0$ has 14.38% more and $[H.C.]_A$

has the highest energy absorption capacity composite. The inclusion of graphene maximized the energy absorption capacity by 14.38%.

2.6.1.3 Notch sensitivity

As per the obtained data, the U-notch gave the least energy absorption capacity while the key hole-notch had 1.16 times more capacity, the V-notch having 1.86 times more capacity and notch free specimen was absorbing maximum energy of 2.63 times more in case of $[NHC]_0$ and it is shown in Figure 2.14. The U-notch gave the least energy absorption capacity while the key hole-notch had 1.17 times more capacity, the V-notch had 1.56 times more capacity, and notch free specimen was absorbing maximum energy of 2.09 times more in the case of $[H.C.]_0$. The U-notch gave the least energy absorption capacity while the key hole-notch had 1.03 times more capacity, capacity, the V-notch had 1.8 times more capacity, and notch free specimen absorbed maximum energy of 2.92 times more in the case of $[H.C.]_A$. The notched specimen has less energy absorption capacity compared with notch free specimen because of stress concentration. Some notch geometry even helps in improvement in impact property as it nullifies the effect of stress concentration caused by the nanoparticle, but some geometry adds stress which results in a decrement in impact strength. The reason for the lower energy absorption capacity for some composite is that when the impactor rebounded, more energy was converted into kinetic energy.

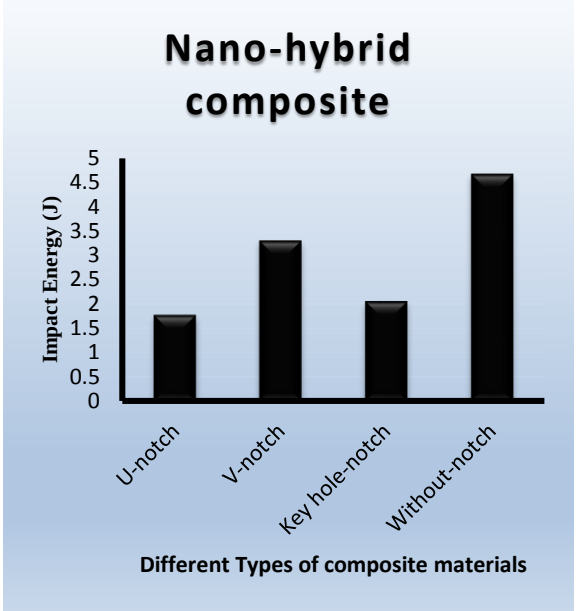

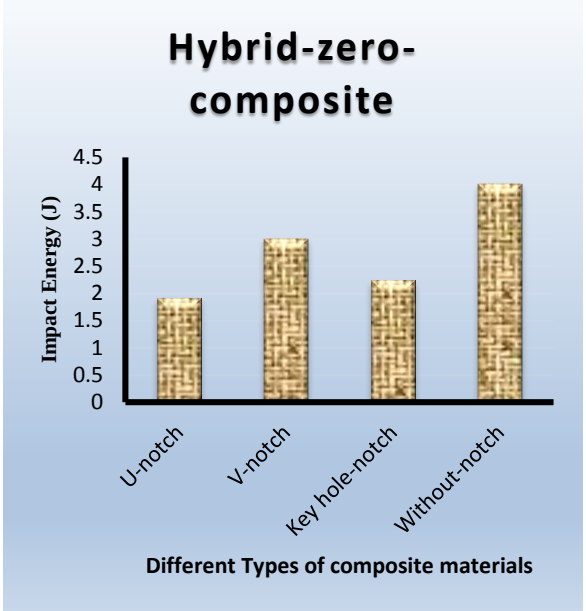

(a) **(b)**

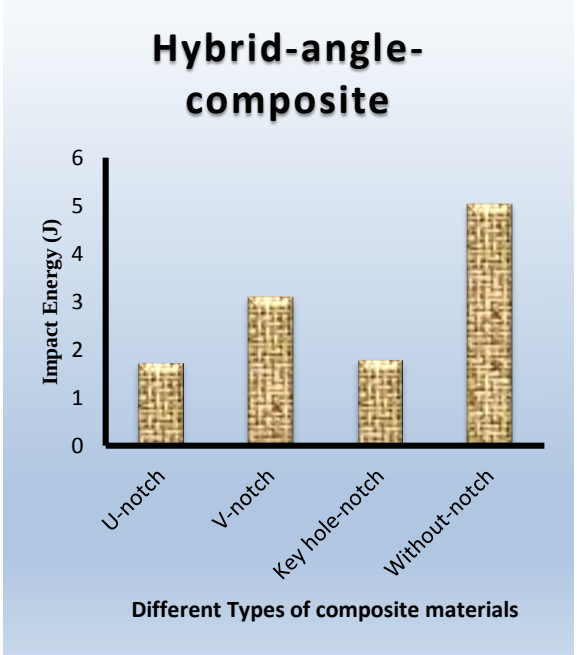

Figure 2.14. Energy absorption charts showing the effect of different notch.

2.6.1.4 Impact strength or resilience

The impact resistance of $[H.C.]_A$ is maximum, followed by $[H.C.]_0$ and $[NHC]_0$ in the case of notch-free and V-notch specimens, whereas in the case of U-notch and key hole-notch, the impact strength of $[H.C.]_0$ is maximum followed by $[H.C.]_A$ and $[NHC]_0$. From Figure 2.15 it is clear that the addition of graphene does not lead to improvement in the impact strength property; it is because of the composite's volume fraction and thickness, which increases the composite's resistance area. The thickness of $[NHC]_0$ is 5mm, whereas, for plain composite, it was 4mm, keeping the other material in the same quantity.

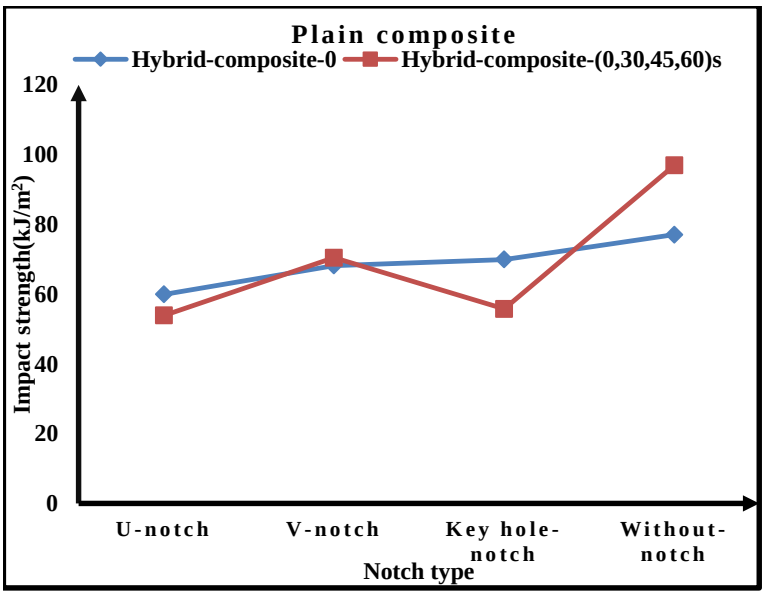

Figure 2.15. Comparison of impact strength of plain composite

The impact energy depends on the amount of material considered during the experiment, and there is not much significant effect of the geometry of notches, but in the case of impact strength, there is a considerable effect of the geometry of notches, as can be seen from Figure 2.15 and Figure 2.16. Keyhole notches use more material during the experiment than U-notch; still, it shows better resistance to fracture in the case of $[H.C.]_A$. The toughness of the composite was influenced by the factors like the addition of graphene powder, fiber type,

fiber sensitivity, fiber orientation and notch sensitivity. The weaving distance between the fibres improves the flexibility of the fiber mat, resulting in an enhancement in impact strength. The impact strength of nanocomposites was lowered due to the individual influence of nano-fillers. However, the combined effect of notches and nanofillers increased the impact strength. This implies that the compatibility of notches and nanofillers is good, which aids in the composite's ability to withstand impact loads and improves the strength. The addition of nano-fillers to nanocomposites improved the matrix's deformation capacity by increasing the surface area of contact between the fillers.

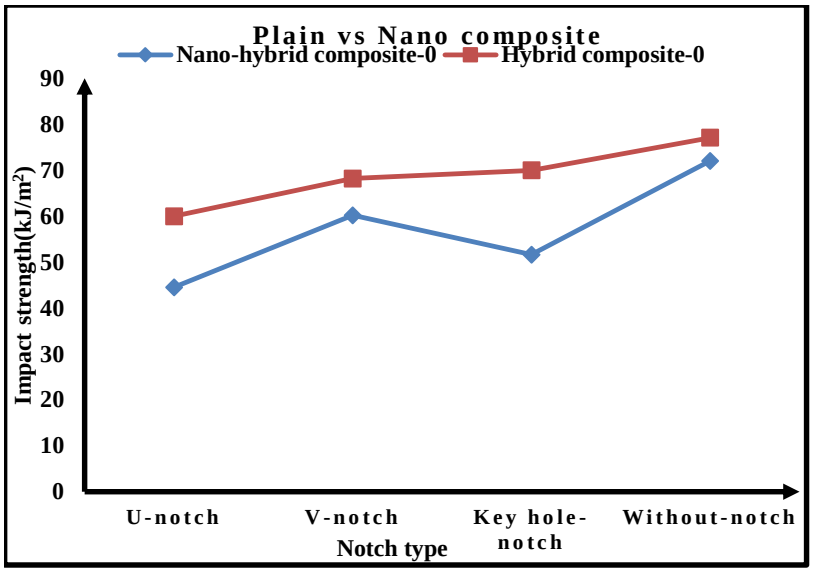

Figure 2.16. Comparison of impact strength of plain composite and Nano composite

Furthermore, the use of nano-filler enhances the synergy between the fillers and hybrid fibres. The addition of nano-fillers improves the energy absorption capacity of the matrix, enhancing the toughness of nanocomposites. As a result, nano-composites show a positive reaction in terms of impact strength. Furthermore, the agglomeration of nano-fillers may reduce the amount of energy needed to affect the material. However, the combined action of both notches- and nano-fillers resulted in a considerable increase in impact strength. An increase

in the stress's localised deformation region causes composites to respond positively. Furthermore, the combined action of notches and nano-fillers reduced stress concentration and regulated hybrid fibre failure, resulting in increased nano-composites impact strength.

2.6.2 Charpy impact

2.6.2.1 Effect of different reinforcement

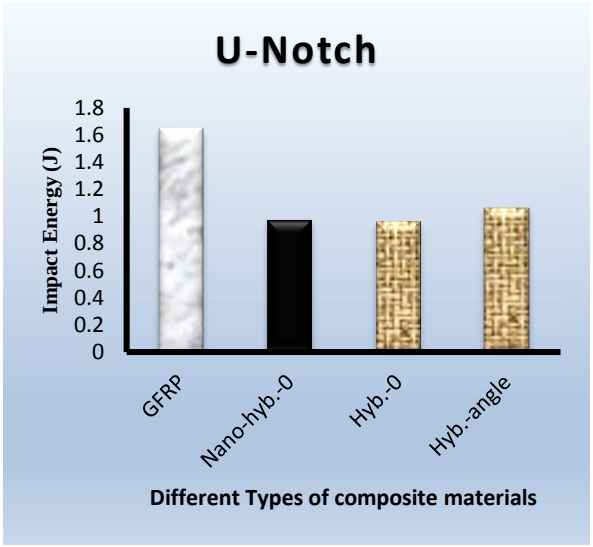

1.4 % increment

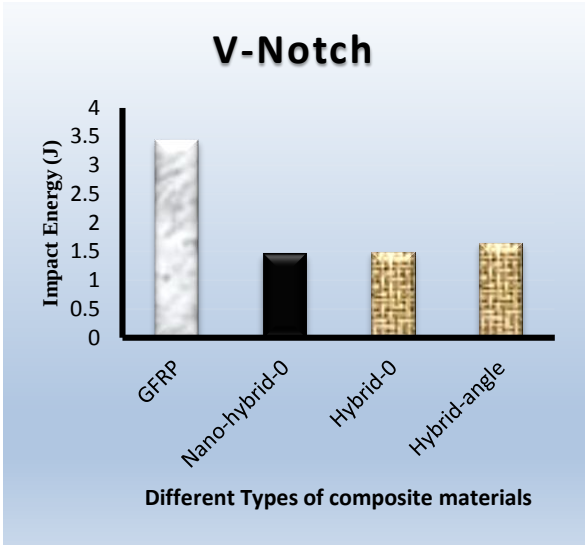

2 % decrement

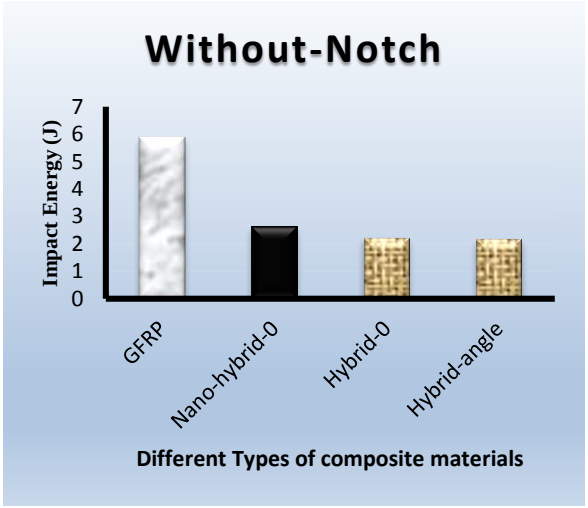

2 % increment

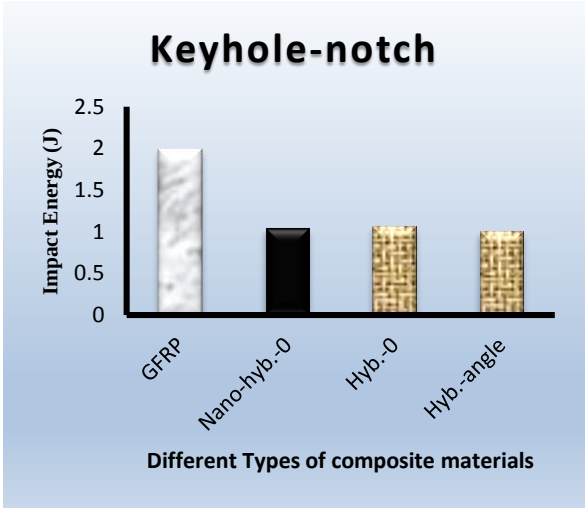

3 % increment

Figure 2.17. Energy absorption charts showing the effect of different reinforcement

One of the most popular methods for rapidly and economically determining a material's relative toughness is the Charpy impact test. The Charpy impact test calculates the energy that a standard notched specimen absorbs when it breaks under impact. Engineering materials such as metals, ceramics, and polymer reinforced composite are still evaluated for their notch sensitivity and impact toughness using this test as an affordable quality control approach. The conventional charpy impact test specimen has dimensions of 127 mm × 12.7 mm × 3.17 mm, and one of the larger dimensions has a notch cut in it. The Charpy impact test determines the amount of energy that a conventionally notched specimen absorbs while breaking under an impact force. An acceptable specimen is held securely at both ends during this test, and a pendulum arm with a hammer is used to strike the specimen. The hammer strikes the surface in the notch's direction. Observing the pendulum arm's slowing down allows one to determine the precise amount of energy that the specimen has received. A material's toughness is greatly influenced by low temperatures, high strain rates, and stress concentrators like notches, cracks, and voids. The calculated results, as shown in Figure *2.17* reveal that $[H.C.]_0$ has the least energy absorption capacity, $[NHC]_0$ has 1.4 % more and GFRP has the highest energy absorption capacity composite in the case of U-notch because composites have stiff and rigid fibres. The inclusion of graphene maximized energy absorption capacity by 1.4 % in the case of U-notch it is because of the presence of nanofillers and the effect of stress concentration. Whereas in the case of V-notch $[NHC]_0$ having the least energy absorption capacity, $[H.C.]_0$ has 2% more than nanocomposites and $[NHC]_0$ is the highest energy absorption capacity composite. The inclusion of graphene minimized the energy absorption capacity by 2% in the case of V-notch; here, notch help nullify the effect of stress concentration, improving energy absorption capacity. In the case of Key hole-notch $[H.C.]_A$ having the least energy absorption capacity, $[NHC]_0$ has 3% less than $[H.C.]_0$ and gfrp has the highest energy absorp

tion capacity. The inclusion of graphene minimized energy absorption capacity by 3 %. In the case of the notch-free specimen, $[H.C.]_A$ has the least energy absorption capacity, $[NHC]_0$ has 2% less than $[H.C.]_0$ and gfrp has the highest energy absorption capacity composite. The inclusion of graphene minimized the energy absorption capacity by 2 %.

2.6.2.2 Notch sensitivity

As per the obtained data, the U-notch gave the least energy absorption capacity while the key hole-notch had 1.1 times more capacity, the V-notch having 1.5 times more capacity and notch free specimen was absorbing maximum energy of 2.7 times more in case of $[NHC]_0$ as given in Figure 2.18. The U-notch gave the least energy absorption capacity while the key hole-notch had 1.1 times more capacity, the V-notch had 1.6 times more capacity, and notch free specimen was absorbing maximum energy of 2.3 times more in the case of $[H.C.]_0$. The key hole-notch gave the least energy absorption capacity while the U-notch had 1.1 times more capacity, the V-notch had 1.6 times more capacity, and notch free specimen absorbed maximum energy of 2.2 times more in the case of $[H.C.]_A$. The notched specimen has less energy absorption capacity compared with notch free specimen because of stress concentration. Some notch geometry even helps in improvement in impact property as it nullifies the effect of stress concentration caused by the nanoparticle, but some geometry adds stress which results in a decrement in impact strength. The reason for the lower energy absorption capacity for some composite is that when the impactor rebounded, more energy was converted into kinetic energy.

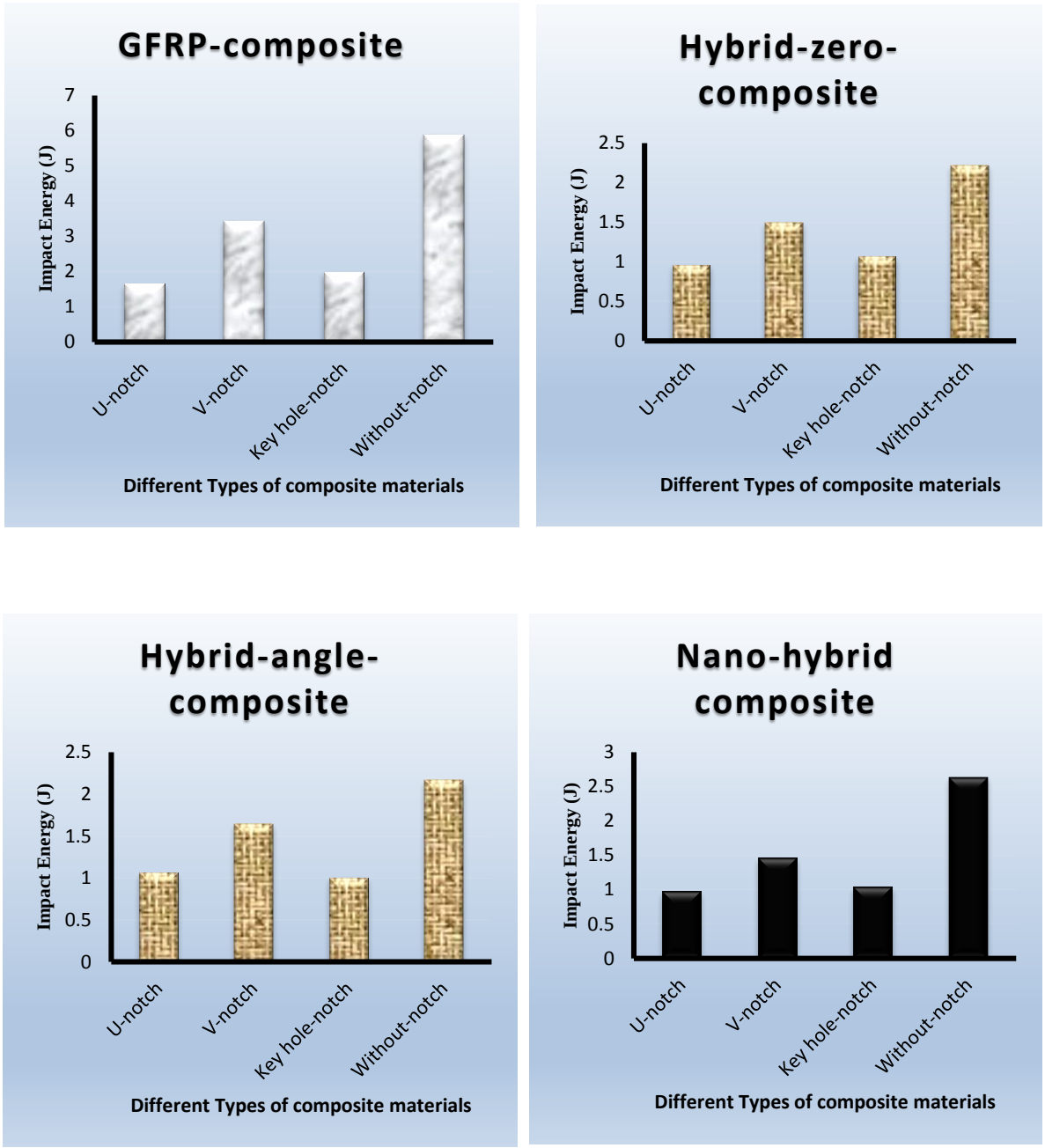

Figure 2.18. Energy absorption charts showing the effect of different notch.

2.7 Machining

2.7.1 Experimental Set-up

The three-axis Micro CNC milling machine set-up was used for slot cutting operation having dimension Length = 15mm; diameter of cutting tool = 2.5mm; depth of cut = 1.05mm.

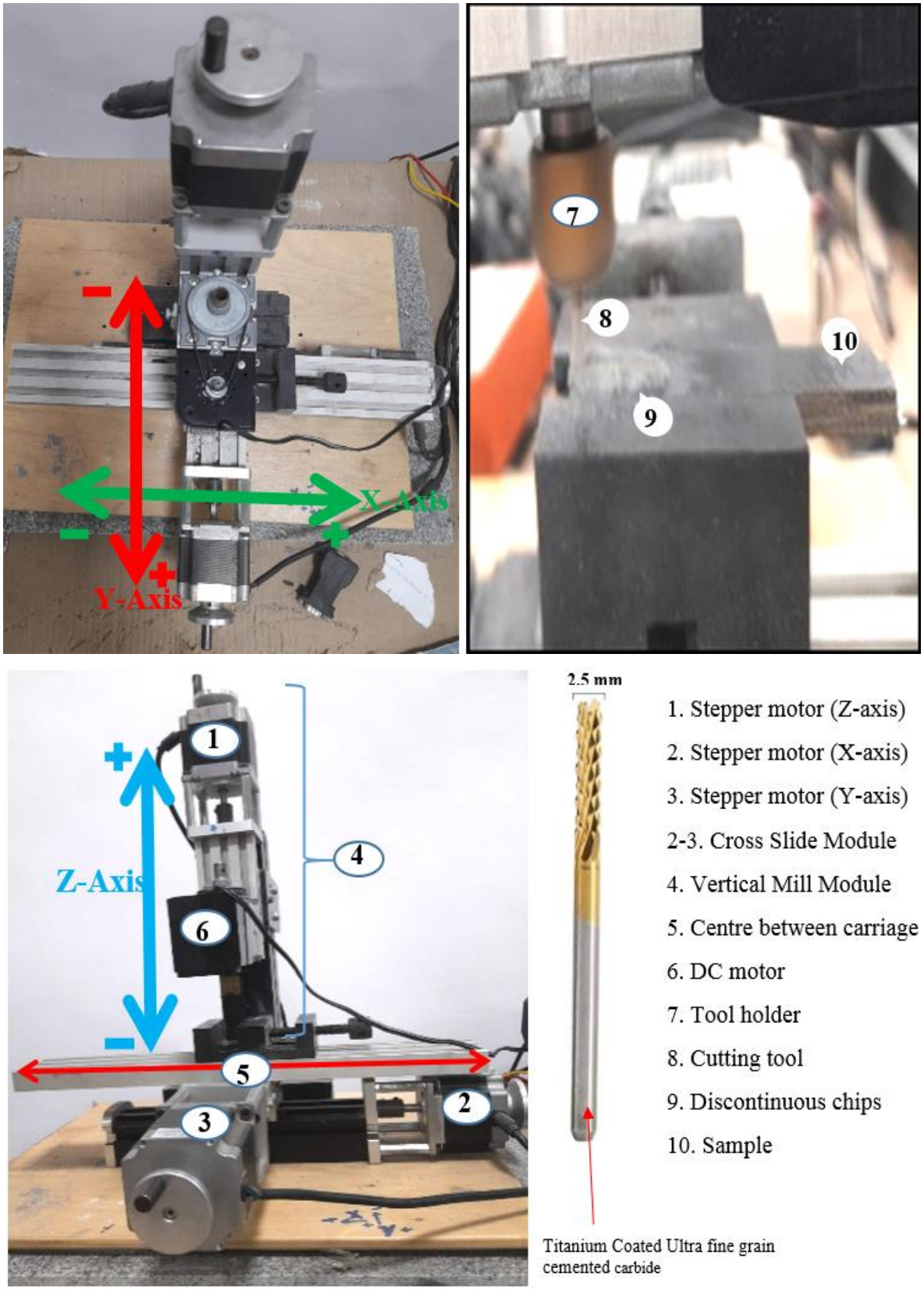

Figure 2.19. 3-axis micro CNC milling machine set-up

The different components of the micromachining set-up are shown in Figure 2.19. The maximum travel of the work table is 145, 50 and 50mm in X, Y, and Z directions, respectively. This machine has a position accuracy of $\pm 5\mu m$ for the entire range and with all three axes and has $\pm 1\mu m$ repeatability for all three axes. For all three axes, the slide is $\pm 1\mu m$ straight. The machine's spindle is driven by a D.C. motor with a speed range of 1220–3461 rpm. All the experiments have been performed on the three axes micro CNC milling machine. This machine consists of four motors, where three motors are used for three axes movement and the 4th one for controlling the speed of the cutting tool. There are a total of ten different speed variations available from 1220 rpm to 4461 rpm. The input parameters are rpm, feed, and material, which were varied, relating one parameter to another to obtain the best output. Input parameters that changed throughout the machining process were Tool speed (rpm), feed (rev/min) and material. Secure the Hybrid composite sample into the holder by tightening the screws of the workpiece holder. The titanium-coated ultra-fine grain cemented carbide rod of 2.5 mm in diameter was used as a cutting tool. The cutting tool was mounted to the spindle, and an N.C. command was used to rotate the spindle. Micrographs showing the micro slots created in the hybrid composite laminates are shown in Figure 2.30.

2.7.2 Experimental Design

The optimal design parameters were determined using the Taguchi L_9 orthogonal array for improved performance and cost [159]. Based on the study reported in the domain of non-conductive materials, the input parameters and their values were chosen [15,41-43]. Each experiment set was repeated at least three times to eliminate any random fluctuation in the experimental results. This method can drastically minimise the number of experiments required, which is essential to get the necessary data. In this investigation, the experimental

plan has cutting speed (rpm), feed and different materials as the governable variable. Based on previous non-conductive material, the various input parameters and levels were identified [40,43–45]. Each trial was performed three times to remove any random fluctuations in the experimental results. Table 2.7 contains a list of the machining input parameters and their levels that were taken into account throughout the experiment. Figure 2.20 depicts the L9 orthogonal array used in the investigation.

Table 2.7. Process variables for nanocomposites at various operating levels.

Input parameter	Level 1	Level 2	Level 3
Tool speed (rpm)	1220	1335	1490
Feed (rev/min)	20	30	40

Table 2.8. Process variables for plain composite at various operating levels.

Input parameter	Level 1	Level 2
Tool speed (rpm)	1335	1490
Feed (rev/min)	20	30
Material	Zero $(0^0,0^0,0^0,0^0)_S$	Angle $(0^0,30^0,45^0,60^0)_S$

The "larger the better" option has opted for the response (MRR). S/N ratios are computed theoretically using equation *(2.5)*. Optimization techniques on the basis of Taguchi method were performed using minitab18

$$\frac{S}{N} = -10log\left[\frac{1}{n}\sum_{i=1}^{n} y_i^2\right] \quad (2.5)$$

Where,

y_i = observed data obtained from experiments

n = number of experiments

2.8 Results and discussion

2.8.1 Taguchi Analysis and ANOVA

The outcomes from the experiments were done by applying Taguchi's L9 orthogonal array Figure 2.20. Our primary target is to increase the MRR, which results in higher productivity, so the S/N ratio can be calculated as "larger the better". The intrinsic influence of input parameters on the MRR is shown in. The relative slope of the linear graph indicates the importance of input parameters. The slope of the graph depicting the influence of feed rate on MRR is clearly higher than that of the other two graphs, as shown in the figure. Hence it can be concluded that the feed rate heavily influences the MRR; tool speed is relatively important, while the material is the least important factor.

Table 2.9. Experimental results of nanocomposites for MRR

Expt. no.	Tool speed (rpm)	Feed (mm/rev.)	MRR (mg/min)	S/N ratio (db)
1	1220	20	3.2205	10.1585
2	1220	30	4.9725	13.9315
3	1220	40	2.4434	7.7599
4	1335	20	3.2349	10.1972
5	1335	30	4.8507	13.7161
6	1335	40	8.7317	18.8220
7	1490	20	2.9203	9.3085
8	1490	30	5.9083	15.4293
9	1490	40	5.7805	15.2393

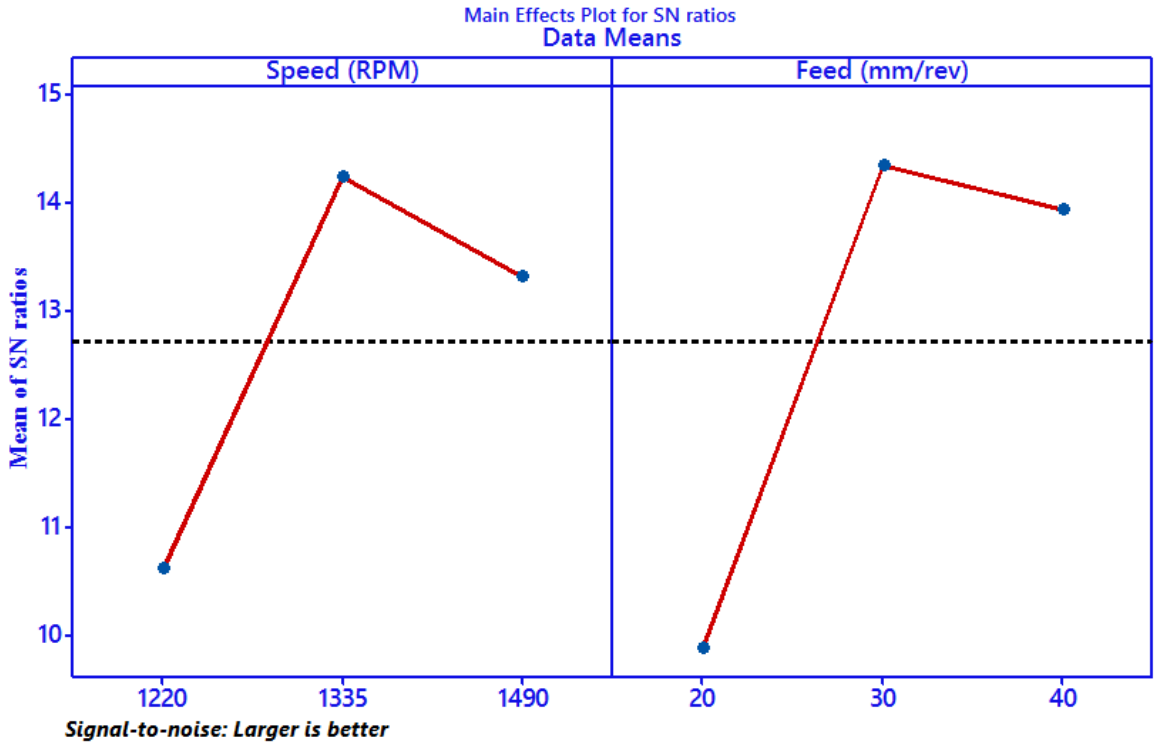

Figure 2.20. Main effect plot for S/N ratios for MRR.

Table 2.10. Response Table for Signal to Noise Ratios (Larger is better)

Level	Speed (RPM)	Feed (mm/rev)
1	10.617	9.888
2	14.245	14.359
3	13.326	13.940
Delta	3.628	4.471
Rank	2	1

2.9 Modeling

In this work, the software programme Minitab 18.0 has been utilised to conduct a linear regression analysis and create a predictive mathematical models for both the dependent parameters material removal rate (MRR) as a function of the cutting speed, feed and materials respectively. Each response has not undergone any modification.

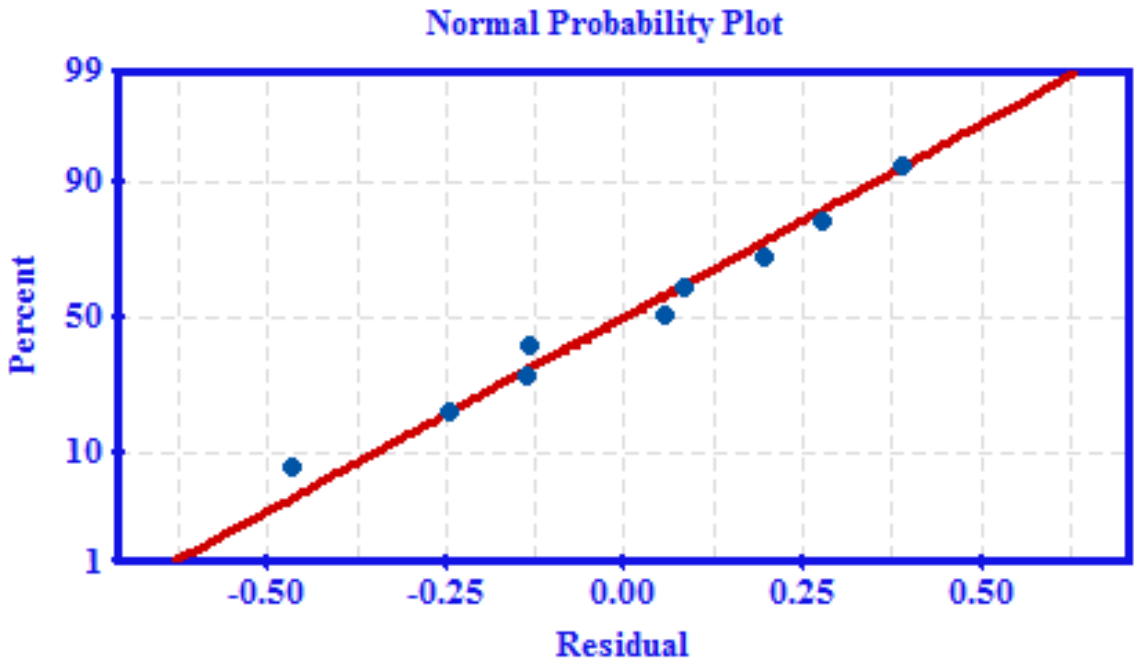

Figure 2.21. Material removal rate residuals shown using a normal probability distribution.

The prediction equations of material removal rate is derived from the regression analysis are summarized in Equation (2.6).

$$MRR\ (mg/min) = 5.32 - 0.00391 \text{ Tool speed (RPM)} + 0.1656 \text{ Feed (mm/rev.)} \quad (2.6)$$

(R^2 = 90.18 %)

Table 2.11. General Linear Model: MRR (mg/min) versus Tool speed, feed and material.

Source	DF	Seq SS	Contribution	Adj SS	Adj MS	F-Value	P-Value
Tool speed (RPM)	2	0.11541	6.53%	0.11541	0.057703	22.23	0.043
Feed (mm/rev.)	2	1.59478	90.22%	1.59478	0.797391	307.19	0.003
Error	2	0.00519	0.29%	0.00519	0.002596		
Total	8	1.76771	100.00%				

It can also be deduced from the graph that the MRR increases as the feed rate increases, owing to the fact that as the feed rate increases, the cutting force increases as well.

Table 2.12. Experimental results of plain composites for MRR.

Expt. no.	Tool Speed (RPM)	Feed (mm/rev)	material	MRR (mg/min)	S/N ratio (db)
1	1335	20	zero	3.81295	11.6252
2	1335	20	angle	3.61960	11.1732
3	1335	30	zero	6.31330	16.0051
4	1335	30	angle	5.38345	14.6212
5	1490	20	angle	3.09700	9.8188
6	1490	20	zero	3.65640	11.2611
7	1490	30	angle	5.41110	14.6657
8	1490	30	zero	5.40185	14.6509

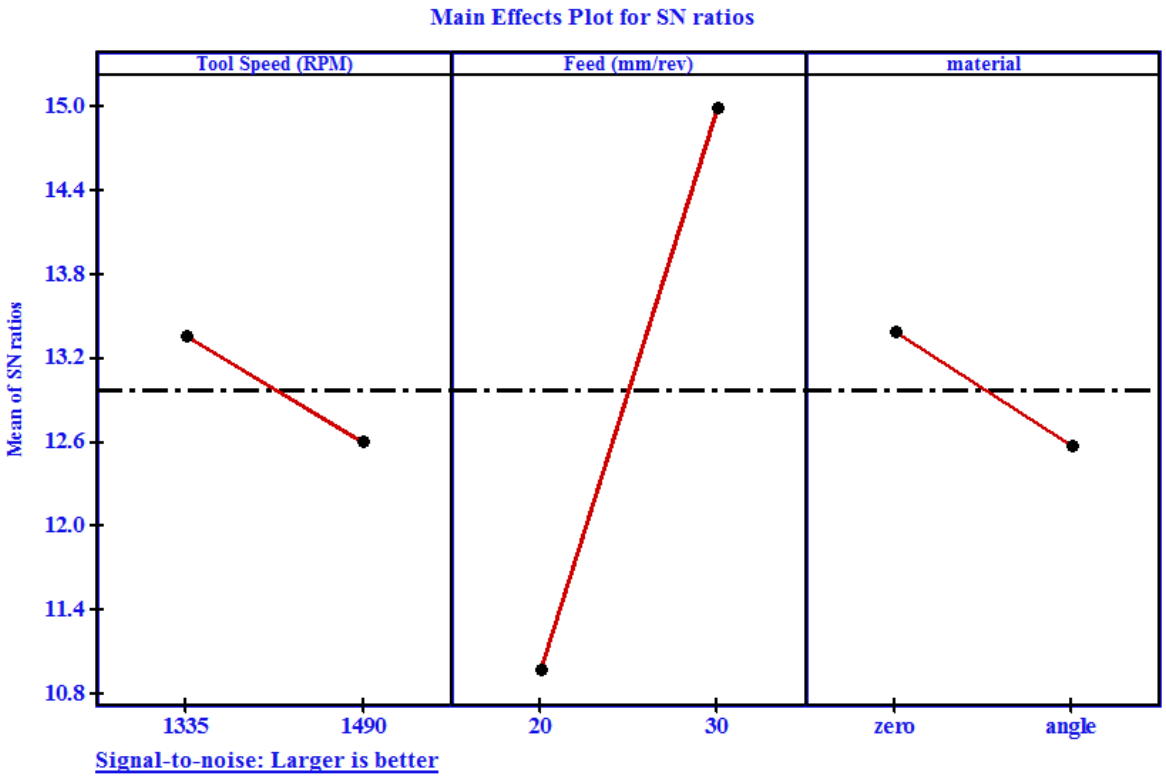

Figure 2.22. Main effect plot of plain composites for S/N ratios for MRR.

Table 2.13. Response Table of plain composites for Signal to Noise Ratios (Larger is better)

Level	Tool Speed (RPM)	Feed (mm/rev)	material
1	13.36	10.97	13.39
2	12.60	14.99	12.57
Delta	0.76	4.02	0.82
Rank	3	1	2

Table 2.14. General Linear Model for plain composites: MRR (mg/min) versus Tool speed, feed and material.

Source	DF	Seq SS	Contribution	Adj SS	Adj MS	F-Value	P-Value
Regression	2	8.96595	93.60%	8.96595	4.48298	36.58	0.001
Tool speed (RPM)	1	0.30535	3.19%	0.30535	0.30535	2.49	0.175
Feed (mm/rev)	1	8.66060	90.42%	8.66060	8.66060	70.67	0.000
Error	5	0.61274	6.40%	0.61274	0.12255		
Lack-of-Fit	1	0.00524	0.05%	0.00524	0.00524	0.03	0.862
Pure Error	4	0.60751	6.34%	0.60751	0.15188		
Total	7	9.57870	100.00%				

MRR reduces as tool spindle speed increases. The cutting force lowers as the tool spindle speed increases because the coefficient of friction decreases as rotational speed increases. This effect is higher at a lower speed, and as the speed increases, this effect is going to decrease. In order to determine the impact of a factor on machining performance, the ANOVA test was used with a 95% confidence level [46,47]. The Fisher test (F-value) has been used to examine the maximum machining parameter values that indicate the most important influencing elements on the process performance. Alternatively, the P-value shows whether a process parameter is significant or not; if the P-value is less than 0.05, then the factor is

significant. shows the analysis of variance for material removal rate. It can be shown that the feed has the maximum percentage contribution to the variance revealed by MRR, followed by tool speed and then material. The low error percentage of 9.82 demonstrates the model's fitness [167]. Figure 2.20. Main effect plot for S/N ratios for MRR. displays the responses for S/N ratios for MRR. The level that shows the highest S/N ratio for each input parameter is the optimum level. Figure 2.20 shows that Level 1 for feed, Level 2 for tool speed, and Level 3 for material are the optimum levels for the highest MRR. The design matrix shows that Exp. No. 8 represents the ideal set of input parameters for MRR. Since the trials were already carried out three times with the ideal input values, there is no need to conduct confirmation experiments. Table 2.15 includes the values of the input parameters at their optimum levels. According to regression analysis, equation (2.6) provides the regression equation for mrr and is used to compute the MRR at the ideal level of input parameters. The results are compared to the experimental data provided in Table 2.16. The maximum of 15% of errors are made. The suitability of the model is determined to be adequate for further research. The conclusion from the analysis of variance in this study might be sent for additional analysis to forecast the optimum setting. When milling hybrid polymer nanocomposites, it can improve the quality of the slot surface. As a result, the ANOVA model has been established in this work.

Table 2.15. Optimum levels of input parameters for response (nanocomposites).

Outcome	Factors	Level explanation	Levels
MRR	Feed (mm/rev.)	30	1
	Tool speed (RPM)	1335	2

Table 2.16. Calculated and experimental values at optimum level (nanocomposites).

Outcome	Claculated	Experimental	%error
MRR	5.5178	6.5068	15

Table 2.17. Optimum levels of input parameters for response (plain composites).

Outcome	**Factors**	**Level explanation**	**Levels**
MRR	Feed (mm/rev.)	30	1
	Tool speed (RPM)	1335	3
	Material	Zero degree	2

Table 2.18. Calculated and experimental values at optimum level (plain composites).

Outcome	Claculated	Experimental	%error
MRR	5.8288	6.3133	7.67

2.10 Response Optimization of the MRR of the hybrid composites

Utilizing contours and 3D plots of RSM, it was possible to assess the interactive relationship between the mix design factors and the properties of plain and nanocomposites. Figure 2.23, Figure 2.24 and Figure 2.25 display the surface plot, contour plot and interaction plot, respectively. Prior to getting the optimum response surface, was used to illustrate the relevance of the major influence of the independent components and their interaction on the outcome that can respond differently by the factors' different levels.

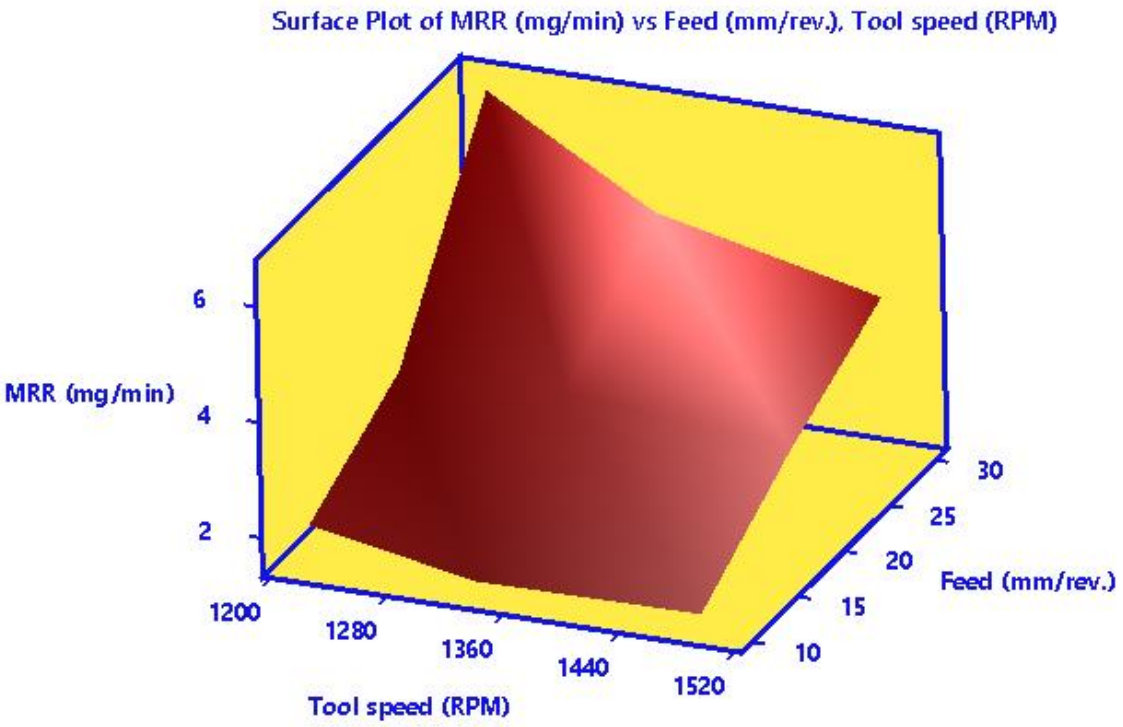

Figure 2.23. Surface Plot of MRR (mg/min) vs feed (rev/min), tool speed (RPM)

As a result, if the outcome exhibits a parallel response to the x-axis, there is no main influence; its significance becomes apparent when the response exhibits a slope behaviour. The magnitude of the major effect grows as this slope increases. The interaction plot illustrates how two separate factors can interact with one another and how this affects the outcome response. If parallel lines are used to represent the factors' impacts on response or duplicate behavior, this means there is no relationship, and hence, there is no interaction between the variables. Only when their curves' slopes vary does the interaction become visible and results in an intersection. In reality, The interaction effect increases as this variation rises [168]. The impact of feed and tool rotational speed and their interaction effect on the material removal rate response of the hybrid composite has shown in Figure 2.25 where both factors significantly influenced the response.

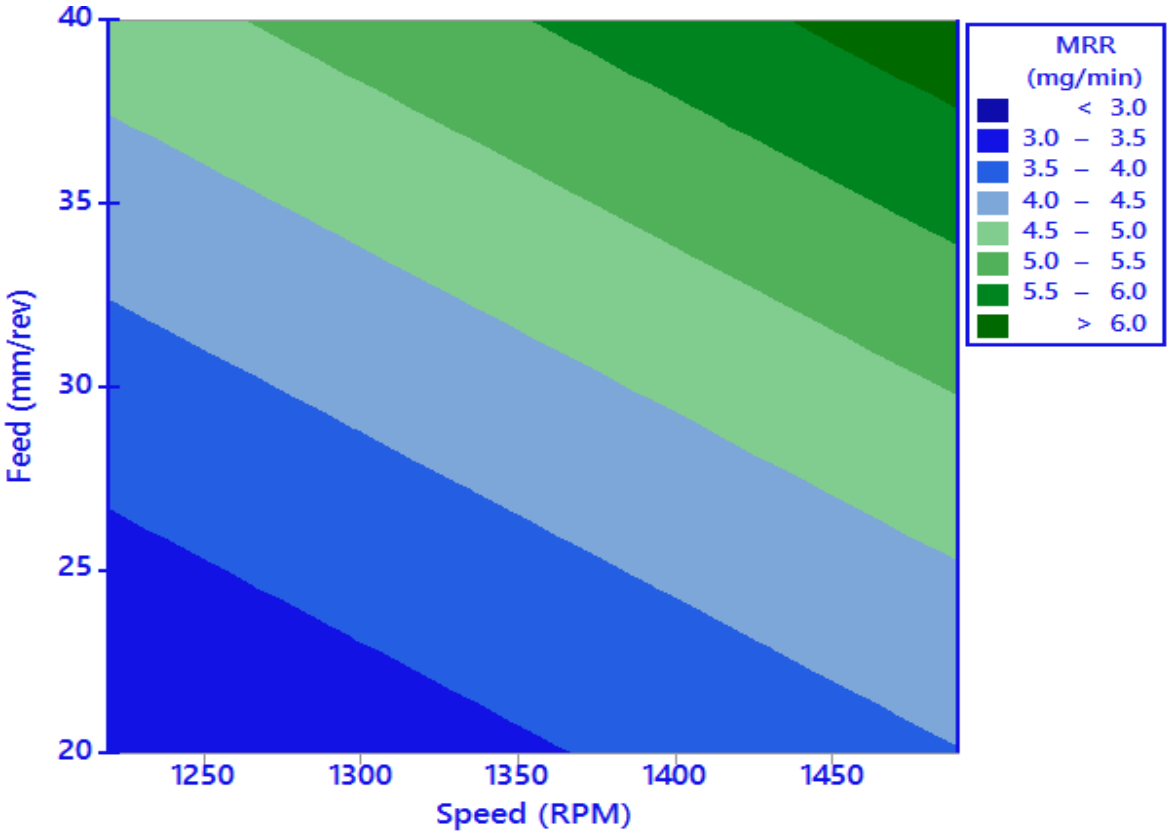

Figure 2.24. Contour Plot of mrr Vs Speed and Feed

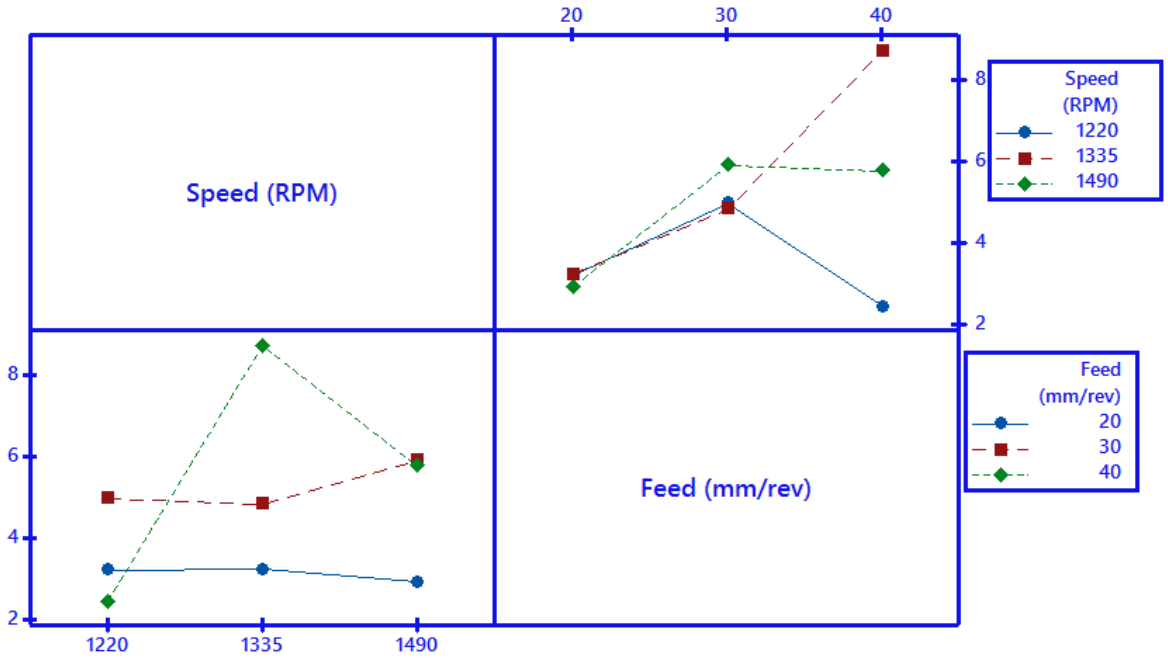

Figure 2.25. Interaction plot of MRR vs Speed, Feed and material.

When compared to tool speed, the feed factor with a steeper slope has a bigger impact on the rate at which material is removed from the workpiece. But as the feed rate approached ten rev/min, this effect nearly disappeared, and a little upturn was seen as a result of the beginning of the phase transition in the epoxy matrix.

2.11 Nano-fillers' effect on the morphology of damaged surfaces

Figure 2.28 depicts the SEM micrograph of tensile failure surface. The fibres are pulled out from the material surface's origin, as seen in the figure. As a result of the filler addition, there

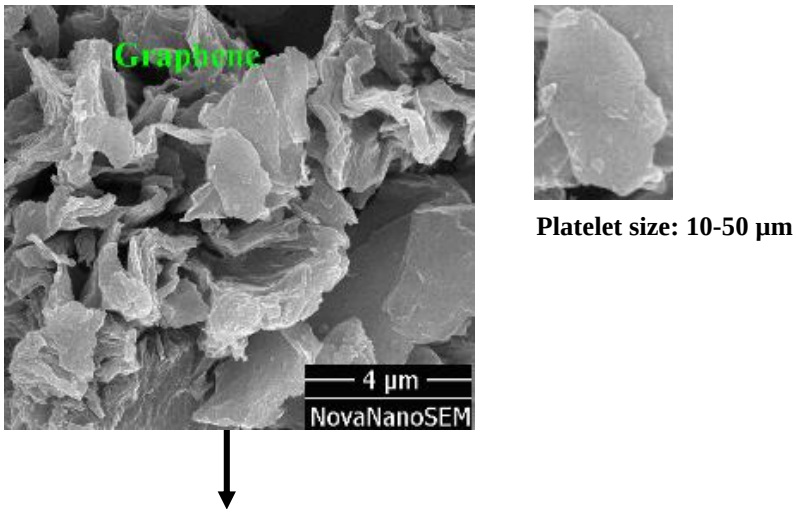

Figure 2.26. SEM image of Reinforcing fillers used in this study. As the size of graphene is smaller therefore there will be evenly distribution in the matrix and the rough surface of graphene ensures better interfacial bonding.

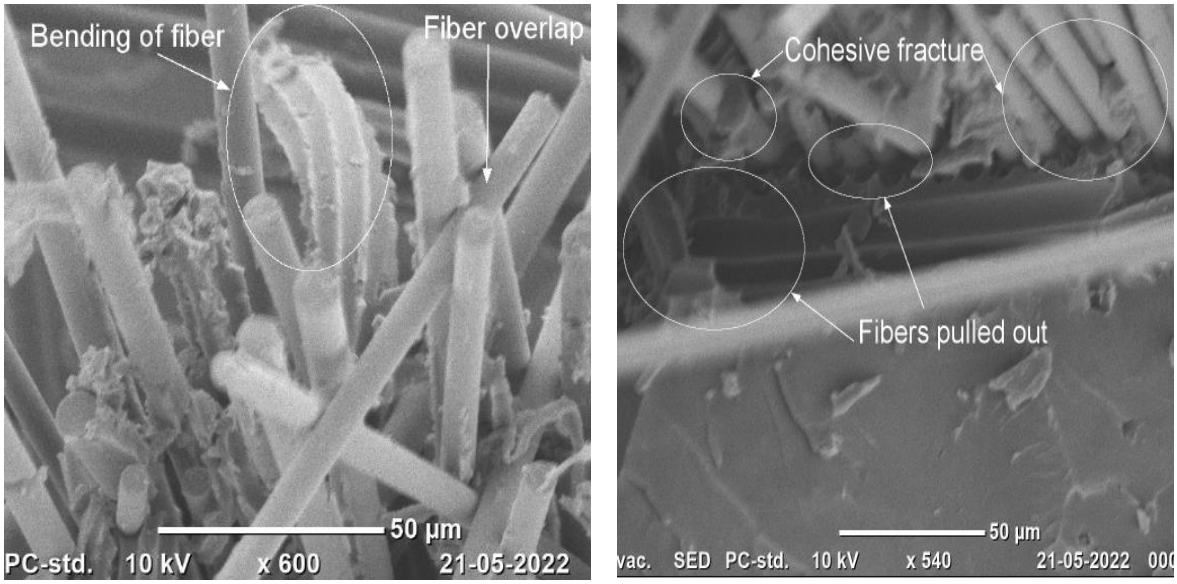

Figure 2.27. SEM image of impact fracture surface of nanocomposites.

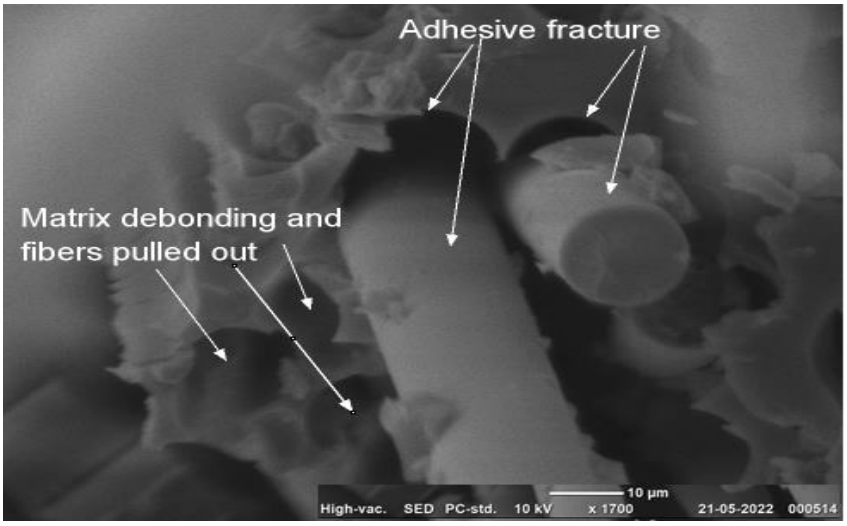

Figure 2.28. SEM image of Tensile fracture surface of nanocomposites

is a localised stress concentration on the material surface. The surface shows agglomeration of fillers as well as matrix deformation. Furthermore, fibre-matrix interface failure (adhesive fracture) has been seen because of the tensile stress concentration in the fibre-matrix interface and [169] noticed the same thing with glass fibres. The roughness of the distorted surface demonstrates the brittleness of the material. The picture shows the imprints of the fibre pulled

out holes. The non-uniform material flow was visible on the failure surface. The use of nano-fillers increases the brittleness of nanocomposite. Figure 2.30 shows the SEM image of the machined surface of nanocomposites.

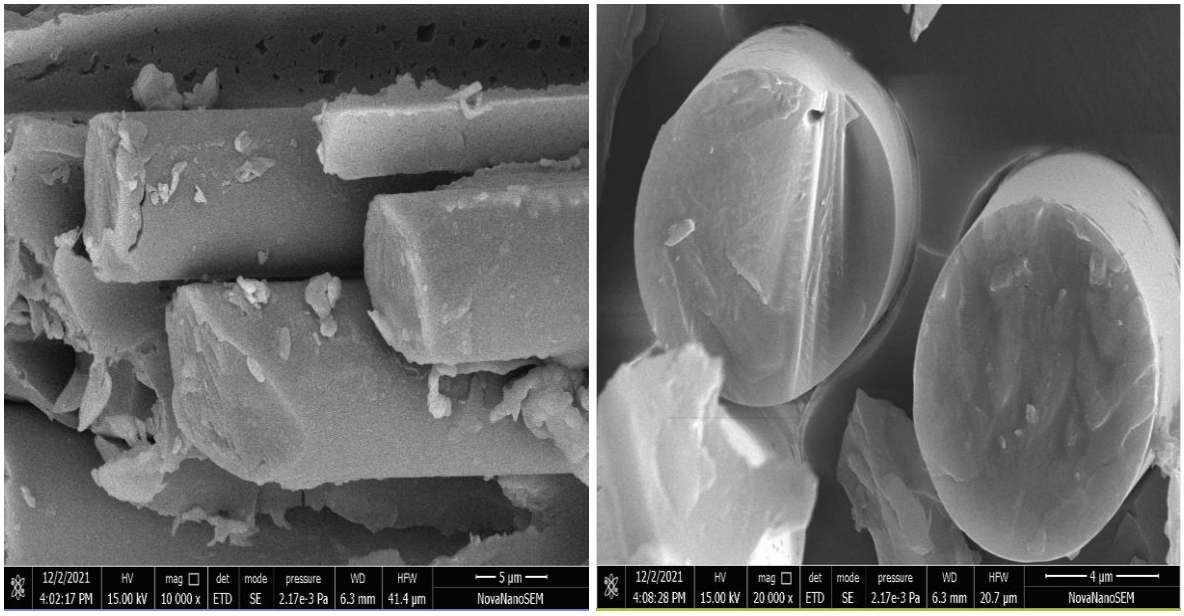

Figure 2.29. . SEM image of Tensile fracture surface of Hybrid composite $(60,45,30,0)_S$.

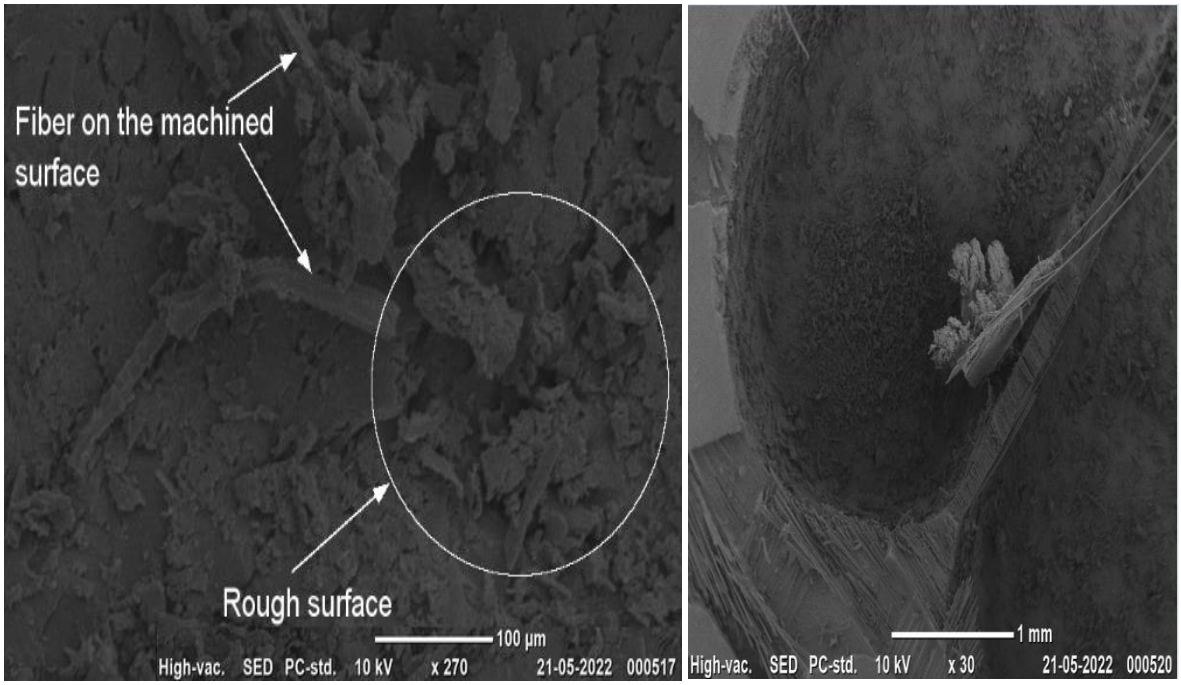

Figure 2.30. SEM image of Machined surface of nanocomposites

Failure takes place because of the presence of microscopic voids, as seen When compared to fracture, the fibre pulled out from the surface is greater [170]. On the failing surface, there are deep voids. This might be related to the hybrid fibre effect. In the process, fibre pull-out devices are ubiquitous. However, the distorted surface revealed that the influence of nano-filler contributed to the deformation's continuation. Furthermore, the stress concentration zone was formed by overlapping the hybrid fibres. The SEM picture of Figure 2.27 shows the morphology of the impact failure surface. Fibre pull-out impressions are more prevalent than fracture impressions, as seen in the figure. Furthermore, the impact has significantly distorted the matrix and fibers. There appears to be a consistent flow of material based on the fracture surface examination. The failure of composites is mostly caused by fibre breakage, the brittle character of the composite and agglomeration of fillers according to the morpho-logical analysis of nanocomposites.

2.12 Conclusion

In comparison to nanocomposite $(0^0,0^0,0^0,0^0)_S$, both hybridcomposite $(0^0,0^0,0^0,0^0)_S$ and $(0^0,30^0,45^0,60^0)_S$ exhibit similar degradative behaviour. However, hybridcomposite samples shows excellent thermal stability, as evidenced by the weight (%) loss of 2.31% for hybrid-composite and 4.77% for nanocomposite from 0^0C to 250^0C. Nanocomposite $(0^0,0^0,0^0,0^0)_S$ material having maximum specific surface area of 2818 m^2/gm which proves that this mate-rial is better adsorbent material compared with other two. The apparent porosity of hybrid-composite $(0^0,30^0,45^0,60^0)_S$ is minimum 6.4 % followed by nanocomposite having 7.9%. Density of nanocomposite is minimum of 1.2185 gm/cm^3. Using a micro CNC milling ma chine, experiments were carried out on hybridcomposite $(0^0,30^0,45^0,60^0)_S$, hybridcomposite

$(0^0,0^0,0^0,0^0)_S$ and nanocomposite $(0^0,0^0,0^0,0^0)_S$ reinforced with graphene platelets fillers. Titanium Coated Ultra fine grain cemented carbide end milling cutter 2.5mm in diameter was employed in all experiments. It is clear from the experimental data that the MRR increases as the feed rate increases. The most crucial variable is the feed rate, followed by cutting speed and different reinforcement materials and also the other parameter such as manufacturing methods, and defects such as weak interfacial bonding, porosity etc. which is affecting the performance. MRR decreases with increasing tool spindle speed. The effect is higher at a lower speed, and as the speed increases, this effect is going to decrease. hybridcomposite $(0^0,30^0,45^0,60^0)_S$ has the highest MRR, followed by hybridcomposite $(0^0,0^0,0^0,0^0)_S$ and nanocomposite $(0^0,0^0,0^0,0^0)_S$. The feed rate, cutting speed, and material all have a big impact on quality loss. It is discovered that the most important variable is the feed rate, followed by cutting speed and different reinforcement materials. Feed rate = 30mm/min, material = Plain composite with ply orientation, and tool speed =1220 rpm produces the optimum material removal rate MRR as 6.5068 mg/min. The experimental MRR (6.5068 mg/min) was close to the calculated MRR (6.612 mg/min) at the optimum input parameter level. The percentage error between the calculated and the experimental value of MRR is very low as 15%. From the ANOVA, it is found that the percentage contributions of the tool rotational speed and feed on MRR are 81.81% and 8.37%, respectively. It is found that there is a reduction in tensile strength by 50.21MPa, and the stiffness is decreased by 23%. The inclusion of graphene minimized energy absorption capacity in the case of U-notch and Key hole-notch. At the same time, it maximized in the case of V-notch and in the case of notch-free specimens. The fractography analysis revealed that mechanical failure is caused by fibre pull-out, fibre-fracture, the crystalline character of composites, and filler agglomeration.